MINISTRY OF HIGHER AND SECONDARY SPECIAL EDUCATION OF THE REPUBLIC OF UZBEKISTAN
TASHKENT STATE TECHNICAL UNIVERSITY NAMED AFTER ISLAM KARIMOV

Mechanics faculty
Department of "Material science"
5320100 – Material science and technology of new materials course group: 81-15

FINAL GRADUATE WORK

Graduation theme: Effects of Mn and V on microstructure and mechanical properties of high-entropy alloys based on AlCoCrNi system.

Head of the department: **DSc. Prof. U.A.Ziyamuxamedova**

Supervisor of graduate student: **Dr. E.E. Jumaev**

Graduate student: **G.B. Abdumanapov**

Tashkent-2019

Contents **Page**

INTRODUCTION

Introduction

Uzbekistan has paid great attention to restoring itself from the first days of independence. Since our country's industries and manufacturing were controlled by the Russian state we didn't develop properly and became dependent on the Soviet system. The first President of the Republic of independent Uzbekistan, I.A.Karimov, managed to save and restore many industries in Uzbekistan for 25 years, to create new industries and attract foreign investors.

The next President of the Republic of Uzbekistan Sh.M.Mirziyoyev continues the development of Uzbekistan, pursuing a full-fledged policy for the development of Uzbekistan. For example, 2018 was announced as a year of "Active business, innovative ideas and support of technology", 2019 was announced as a year of "Active investment and social development". Furthermore, we can tell that by implementing this policy a number of new enterprises have been created, such as: construction of the second gas-fired power plant at "Navoi Thermal Power Station", sale of "Fergana Oil Refinery" to foreign investors, implementation of 31 investment projects in "Chemical Industry", reorganization of "Uzbekenergo", implementation of major projects in "Navoiazot", establishment of "Marmarobod" enterprise, launch of the "Thermal Power Station" in Turakurgan, construction of a large chemical complex "Manufacturing of Mineral Fertilizers" in Syrdarya, construction of "Nuclear Power Plants", construction of the "Ustyurt Gas-Chemical Complex" basis in Surgil and others.

Moreover, many treaties and agreements were signed with other developed countries on the path of development of our country. For example, we can say that during the visit of Korean President, Moon Zhe Ying, on April 18-21 to our contry, Uzbekistan and Korea signed agreements on implementation of joint projects and programs worth over 12 billion US dollars in trade, economy, investment, finance and other technical fields. This agreement includes: encouragement and mutual protection of investments between the government and the ministries, exploration of space for peaceful purposes, cooperation in science, technology and innovation,

establishment of the Uzbek-Korean center for healthcare cooperation and other documents. The search for new opportunities, including the development of information and communication technologies, the fifth generation of 5G mobile communication technologies, space technologies, new industries, in particular, medicine and the importance of expanding cooperation in promising areas such as bioindustry and others were emphasized by Korean President Moon Zhe Ying as vital areas to widen our cooperation.

SECTION I

SPECIAL SECTION

Special section

1.1. Beginning part

Man, through the ages, has undergone many changes from the time when he depicted a herd of mammoths on the walls of his cave to these days when he can create beautiful pictures and even make coffee by use of computer technologies without leaving his favorite chair.

The 21st century made huge steps in developing computer technologies, mechanical engineering, aircraft building and other areas and reached many goals that made our life much easier.

The most developing technologies in our life are connected one way or another with new materials. If people wish to create something new they have to choose the right material. So, nowadays we are using alloys (high-entropy alloys) where they are replaced with a range of metals with better features.

Human civilization progresses as materials progress. Metal Age comprises Bronze Age and Iron Age and spans about five thousand years till now. Even in this new Silicon Era which came into being just several decades ago, we still rely largely upon metals, especially upon high-performance metals. It is interesting to note that most high-performance metals were developed in the last 150 years. This is a very short period compared with the whole Metal Age.

Up until 1970s, almost all traditional alloys were developed and provided a wide spectrum of properties and performances. There have been about 30 commonly used traditional alloy systems, including steel, aluminum, copper, etc. as seen in the ASM (American Society for Metals) metals handbooks. However, they were still unsatisfactory in many aspects of application. Therefore, many efforts have been made to develop new metals in the last four decades. Three routes are chosen for this approach: to create new compositions, to invent new processes, and to use new combinations of composition and process. Thus, intermetallics, metal-matrix composites, metallic glasses, thermomechanical processing, rapid solidification, mechanical alloying, spray deposition, equal-channel angular pressing, reciprocating extrusion, superplastic forming, nanotechnology, etc. were

proposed and investigated. Even so, there still exist many bottlenecks to overcome since the requirements for high performance become more and more strict in most applications.

When examining the design concept for traditional alloys, it can be found that almost all alloys are based on one principal metallic element and seldom have more than three principal metallic elements. For example, steel is based on iron; superalloys might be based on Ni, Co, or Fe; intermetallics are based on Ni-Al compounds, Ti-Al compounds, Fe-Al compounds, etc.; metal-matrix composites might be based on Ni, Ti, or Al; and metallic glasses have nine different bases: Pd-, Mg-, Ln-, Zr-, Ti-, Cu-, Fe-, Co-, and Ni-base. Thus, under the traditional concept, metallurgists make and process alloys, study their microstructure and properties, and provide them for suitable applications. Obviously, the degrees of freedom in alloy development are confined by this alloy concept. At the end of the last century, the development of new metals became mature and reached its limit.

1.2. Investigating part

Based on physical metallurgy and experience, people are easy to have a misunderstanding that HEAs would contain many intermetallic compounds and become too brittle to be applicable. However, the experimental evidences have revealed that high entropy would enhance the formation of more ductile solid-solution phases and thus simplify the microstructure. XRD analyses shows of as-cast $Al_xCoCrCuFeNi$ alloy system with different x values in molar ratio. The major phases are FCC and BCC. As x exceeds 0.8, increasing aluminum content increases the volume fraction of BCC and ordered BCC (B2) phases, and spinodal decomposition of BCC or B2 phase occurs around 600°C.

For one more example, x-ray shows diffraction patterns of binary to 7-element equimolar alloys demonstrating the microstructure simplicity. The six alloys were prepared with the arc melting method by adding one element in the sequence of Cu-Ni-Al-Co-Cr-Fe-Si. It reveals that their constituent phases do not become complicated as the number of elements increases. The major phases are also BCC and FCC. Moreover, all peak intensities decrease as the number of elements

increases indicating the lattice distortion increases or crystallinity decreases. The 6-element equimolar alloy AlCoCrCuFeNi is chosen for illustrating the phase simplicity. There is 44 possible binary intermediate phases found in binary phase diagram, most being compounds. Obviously, there are more possible ternary phases for this alloy. However, all these phases are actually inhibited and BCC and FCC phases are the main phases. In addition, the number of phase is significantly lower than the maximum number of phases predicted by the Gibbs phase rule.

To emphasize the simple solid-solution phases formed, several compositions ($\geq$5 principal elements) and processes including conventional casting, sputtering, and splat-quenching were used to produce the single-phase microstructure as revealed by the XRD patterns. This indicates that multi-principal elements could form solid solutions with a simple FCC or BCC crystal structure. That is, all different atoms are regarded as solutes and expected to randomly distribute (or at most slight short-range ordering) in the crystal lattices under the occupancy probability of a statistical average without a "matrix or host" element defined. Therefore, we proposed the concept of extended crystal structure. The point is that conventional crystal structure can be extended for multi-principal elements.

1.3. Final part

To overcome this constraint, I proposed a new approach "high-entropy alloys" for alloy design and started to explore this new alloy field. High-entropy alloys are defined to have at least 5 principal metallic elements, each of which has the atomic percentage between 5 % and 35 %. For example, we could have a 6-element equimolar alloy as AlCoCrNiVMn and a nonequimolar alloy as $(AlCoCrNi)_{84}V_8Mn_8$. Furthermore, we might modify the alloys with minor elements such as $AlCo_{0.5}CrCuFe_{1.5}Ni_{1.2}B_{0.1}C_{0.15}$. With this brand new concept of alloy design, a huge number of new alloys could be designed and studied, and many new phenomena, new properties, and new applications could be discovered.

In my study, I conclude that high-entropy alloys could be made, processed and analyzed like conventional alloys. Moreover, they exhibit several interesting features as reported in the previous researches:

1. Tend to form simple solid solution phases such as BCC and B2 with nanostructures.
2. Range from HV100 to HV1500 in hardness.
3. Have a good thermal stability in microstructure.
4. Deform under a nano-twinning deformation mechanism.
5. Have an excellent resistance to anneal softening.
6. Could have a high-temperature precipitation hardening between 600 and 1000°C.
7. Could have a positive temperature coefficiently of strength and hence maintain a high strength level at elevated temperatures.

Thanks to these special properties, they have many potential applications.

- First application: tools, molds, dies, mechanical parts and furnace parts requiring properties of high strength, thermal stability, wear and oxidation resistances;

- Second: anticorrosive high-strength materials in chemical plants, IC (Integrated Circuit) foundries, and even marine applications for piping and pump components requiring excellent corrosion resistance;

- Third: they could be produced as functional films such as hard-facing of golf heads and rolls, hard and anti-sticky coating for molds and tools, diffusion barrier for Cu interconnection in ultra large-scale integrated circuits, and soft magnetic films for ultra-high-frequency communication.

In this diploma work, the effect of Mn and V on microstructure and mechanical properties of AlCoCrNi high-entropy alloy are reviewed and their tendency to form simple microstructure with nanostructure and basic microstructural features discussed.

SECTION II

GENERAL INFORMATION ABOUT HIGH-ENTROPY ALLOYS SYSTEM

General information about high-entropy alloys system

Recently, high-entropy alloys (HEAs) have attracted increasing attention because of their unique compositions, microstructures, and adjustable properties. They are loosely defined as solid solution alloys that contain more than five principal elements in equal or near equal atomic percentage (at.%). Normally, the atomic fraction of each component is greater than 5 at.%. The multi-component equi-molar alloys should be located at the center of a multi-component phase diagram, and their configuration entropy of mixing reaches its maximum (R Ln N; R is the gas constant and N the number of component in the system) for a solution phase. These alloys are defined as HEAs by Yeh entropy alloys and named by Cantor entropy alloys as multi-component alloys. Both refer to the same concept. There are also some other names, such as multi-principal-elements alloys, equi-molar alloys, equi-atomic ratio alloys, substitutional alloys, and multi-component alloys.

Cantor entropy alloys pointed out that a conventional alloy development strategy leads to an enormous amount of knowledge about alloys based on one or two components, but little or no knowledge about alloys containing several main components in near-equal proportions. Theoretical and experimental works on the occurrence, structure, and properties of crystalline phases have been restricted to alloys based on one or two main components. Thus, the information and understanding are highly developed on alloys close to the corners and edges of a multi-component phase diagram, with much less knowledge about alloys located at the center of the phase diagram, as shown schematically for ternary and quaternary alloy systems in Fig. 1. This imbalance is significant for ternary alloys but becomes rapidly much more pronounced as the number of components increases. For most quaternary and other higher-order systems, information about alloys at the center of the phase diagram is virtually nonexistent except those HEA systems that have been reported very recently.

In the 1990s, researchers began to explore metallic alloys with super-high glass-forming ability (GFA). Greer proposed a confusion principle, which states that the more elements involved, the lower the chance that the alloy can select viable crystal structures, and thus the greater the chance of glass formation. Ma entropy alloys found that the best glass former is not exactly at the eutectic composition, and has a shift towards the high-entropy zone in the phase diagram. Recently, Takeuchi entropy alloys reported a high-entropy bulk metallic glass (BMG), which can have a critical size over 10 mm. Zhao entropy alloys and Gao entropy alloys reported a high-entropy BMG, which can be plastically deformed at room temperature. However, for some HEAs, their GFA is rather low, and they can only form solid-solutions even though the cooling rate is very high, e.g., alloys of CuCoNiCrAlFeTiV, FeCrMnNiCo, CoCrFeNiCu, AlCoCrFeNi, NbMoTaWV, etc.

The yield strength of the body-centered cubic (BCC) HEAs can be rather high usually comparable to BMGs. Moreover, the high strength can be kept up to 800 K

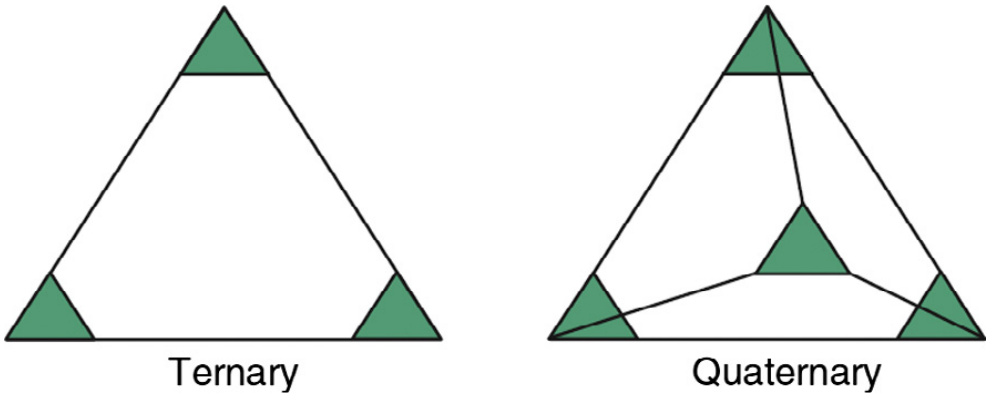

Fig. 1. Schematic ternary and quaternary alloy systems, showing regions of the phase diagram that are relatively well known (green) near the corners and relatively less well known (white) near the center.

or higher for some HEAs based on 3d transition metals. In contrast, BMGs can only keep their high strength below their glass-transition temperature.

2.1. Four core effects

Being different from the conventional alloys, compositions in HEAs are complex due to the equi-molar concentration of each component. Yeh summarized mainly four core effects for HEAs, that are:

- Thermodynamics: high-entropy effect;

- Kinetics: sluggish diffusion;
- Structures: severe lattice distortion;
- Properties: cocktail effect.

I will discuss these four core effects separately.

High-entropy effect.

The high-entropy effect, which tend to stabilize the high-entropy phases, e.g., solid-solution phases, were firstly proposed by Yeh. The effects were very counterintuitive because it was expected that intermetallic compound phases may form for those equi- or near equi-atomic alloy compositions which are located at the center of the phase diagrams (for example, a monoclinic compound AlCeCo forms in the center of Al–Ce–Co system). According to the Gibbs phase rule, the number of phases (P) in a given alloy at constant pressure in equilibrium condition is:

$$P = C + 1 - F$$

where C is the number of components and F is the maximum number of thermodynamic degrees of freedom in the system. In the case of a 6-component system at given pressure, one might expect a maximum of 7 equilibrium phases at an invariant reaction. However, to our surprise, HEAs form solid-solution phases rather than intermetallic phases. This is not to say that all multi-components in equal molar ratio will form solid solution phases at the center of the phase diagram. In fact, only carefully chosen compositions that satisfy the HEA-formation criteria will form solid solutions instead of intermetallic compounds.

The solid-solution phase, according to the classical physical-metallurgy theory, is also called a terminal solid solution. The solid-solution phase is based on one element, which is called the solvent, and contains other minor elements, which are called the solutes. In HEAs, it is very difficult to differentiate the solvent from the solute because of their equi-molar portions. Many researchers reported that the multi-principal-element alloys can only form simple phases of body-centered-cubic (BCC) or face-centered-cubic (FCC) solid solutions, and the number of phases formed is much fewer than the maximum number of phases that the Gibbs phase rule allows. This feature also indicates that the high entropy of the alloys tends to

expand the solution limits between the elements, which may further confirm the high-entropy effects.

The high-entropy effect is mainly used to explain the multi-principal-element solid solution. According to the maximum entropy production principle (MEPP), high entropy tends to stabilize the high-entropy phases, i.e., solid-solution phases, rather than intermetallic phases. Intermetallics are usually ordered phases with lower configurational entropy. For stoichiometric intermetallic compounds, their configurational entropy is zero.

Whether a HEA of single solid solution phase is in its equilibrium has been questioned in the scientific community. There have been accumulated evidences to show that the high entropy of mixing truly extends the solubility limits of solid solution. For example, Lucas entropy alloys recently reported absence of long-range chemical ordering in equi-molar FeCoCrNi alloy that forms a disordered FCC structure. On the other hand, it was reported that some equi-atomic compositions such as AlCoCrCuFeNi contain several phases of different compositions when cooling slowly from the melt, and thus it is controversial whether they can be still classified as HEA.

Sluggish diffusion effect

The sluggish diffusion effect here is compared with that of the conventional alloys rather than the bulk-glass-forming alloys. Recently, Yeh studied the vacancy formation and the composition partition in HEAs, and compared the diffusion coefficients for the elements in pure metals, stainless steels, and HEAs, and found that the order of diffusion rates in the three types of alloy systems is shown below:

HEAs < stainless steels < pure metals

The sluggish diffusion effect is usually used to explain the formation of nano-sized precipitations, because the nuclei are easier to form but grow slowly, as shown in Fig. 2 on an as-cast CuCoNiCrFe alloy. In the figure, nano-precipitates with a size of 7–50 nm in diameter, close to the FCC phase in a spinodal plate appear, as shown in Fig. 2B(b). Fig. 2 also shows that the microstructures of certain HEAs are

usually very complicated, which can include nano-precipitates, ordered solid solution phases, disordered solid-solution phases, and even amorphous phases. This feature is due to the fact that the interactions between the principal elements and the content of all the elements are very high.

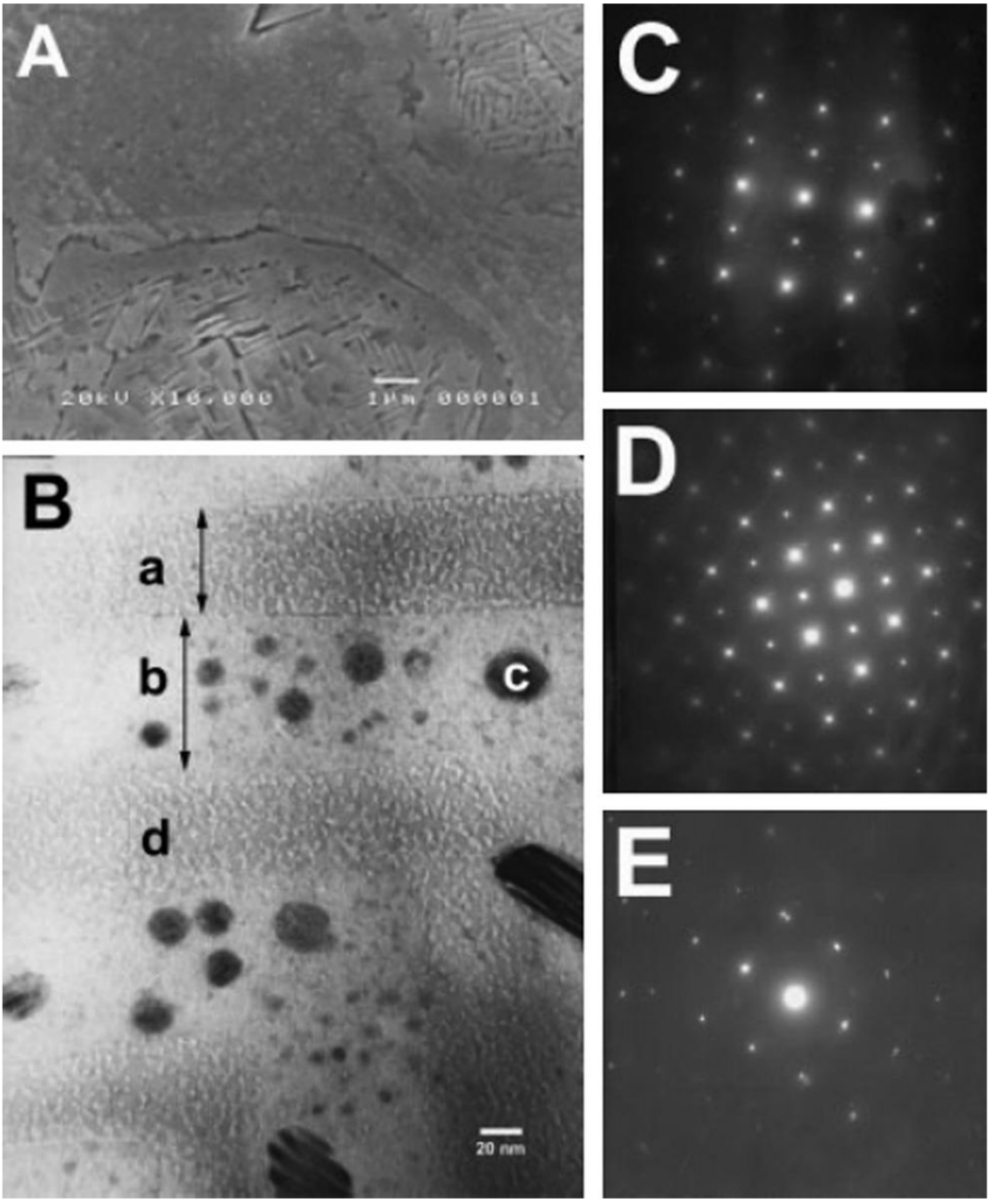

Fig. 2. Microstructures of an as-cast CuCoNiCrAlFe alloy. (A) SEM micrograph of an etched alloy with dendrites (a spinodal structure of disordered BCC and ordered BCC phases) and interdendrite (an FCC phase) structures. (B) TEM bright-field image; (B-a) an inter-spinodal plate, 70-nm wide, a disordered BCC phase (A2), lattice constant, 2.89A; (B-b) a spinodal plate, 100-nm wide, an ordered BCC phase (B2), lattice constant, 2.89A; (B-c) nanoprecipitation in a spinodal plate, 7 nm to 50 nm in diameter, close to the FCC phase; (B-d) nanoprecipitation in an interspinodal plate, 3 nm in diameter, a disordered BCC phase (A2). (C–E) Corresponding selected area diffraction (SAD) patterns of B, Ba, and Bb with zone axes of BCC, BCC superlattice, and FCC, respectively.

Severe lattice-distortion effect

The severe lattice-distortion effect is usually compared with the one dominant element alloys, where the lattice site is occupied mainly by the dominant constituent. For HEAs, each element has the same possibility to occupy the lattice site, if ignoring chemical ordering. Since the size of different elements can be very different in some cases, this can lead to the severe lattice distortion. This effect is well confirmed by the ultrahigh strength of the BCC HEAs. Yeh entropy alloys studied the anomalous decrease in X-ray diffraction (XRD) intensities of the CuNiAlCoCrFeSi alloy systems with multi-principal elements. A series of CuNiAlCoCrFeSi alloys with a systematic addition of principal elements from pure element to seven elements was investigated for the quantitative analysis of XRD intensities. The variation of XRD peak intensities of the alloy system is similar to that caused by thermal effects, but the intensities further drop beyond the

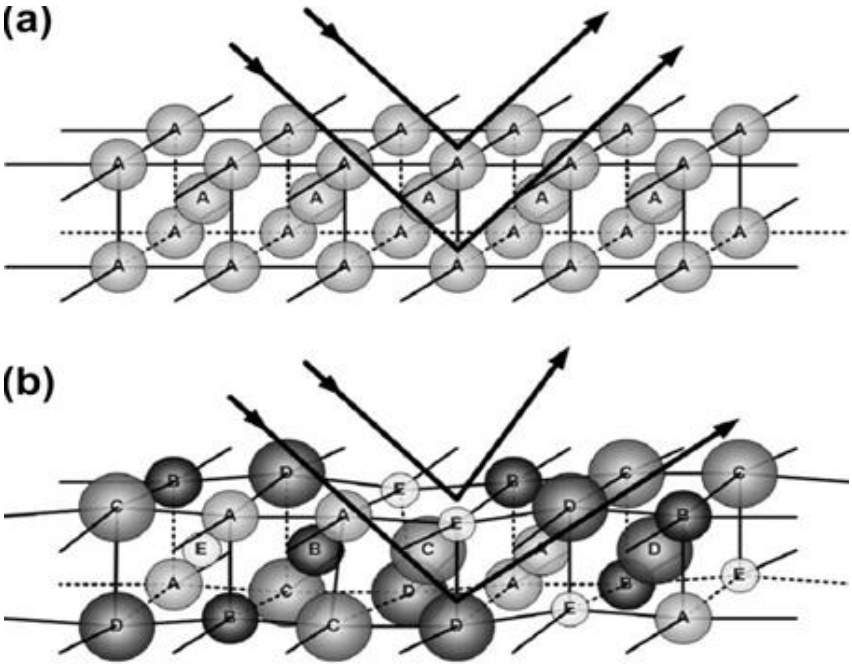

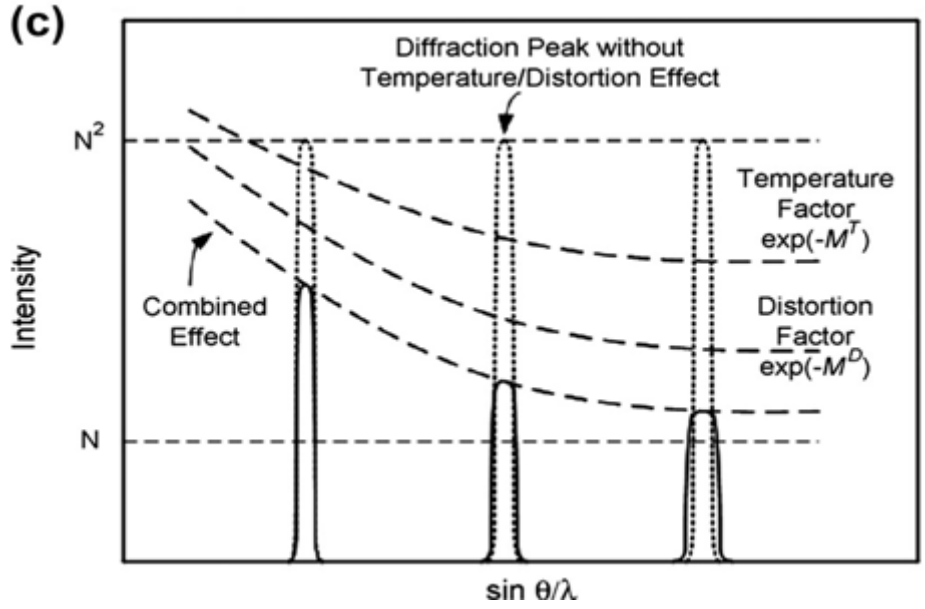

Fig. 3. Schematic illustration of intrinsic lattice distortion effects on Bragg diffraction: (a) perfect lattice with the same atoms; (b) distorted lattice with solid solutions of different-sized atoms, which are expected to randomly distribute in the crystal lattice according to a statistical average probability of occupancy; (c) temperature and distortion effects on the XRD intensity.

thermal effect with increasing the number of constituent principal elements. An intrinsic lattice distortion effect caused by the addition of multi-principal elements with different atomic sizes is expected for the anomalous decrease in the XRD intensities. The mathematical treatment of this distortion effect for the modification of the XRD structure factor is formulated to be similar to that of the thermal effect, as shown in Fig. 3. The larger roughness of the atomic planes makes the intensity of the XRD for HEAs much lower than that for the single-element solid.

The severe lattice distortion is also used to explain the high strength of HEAs, especially the BCC-structured HEAs. The severe lattice-distortion effect is also related to the tensile brittleness and the slower kinetics of HEAs. However, the authors also noticed that single-phase FCC-structured HEAs have very low strength, which certainly cannot be explained by the severe lattice distortion argument. Fundamental studies in quantification of lattice distortion of HEAs are needed.

Cocktail effect

The cocktail-party effect was usually used as a term in the acoustics field, which have been used to describe the ability to focus one's listening attention on a single talker among a mixture of conversations and background noises, ignoring

other conversations. For metallic alloys, the effect indicates that the unexpected properties can be obtained after mixing many elements, which could not be obtained from any one independent element. The cocktail effect for metallic alloys was first mentioned by Ranganathan, which has been subsequently confirmed in the mechanical and physical properties.

The cocktail effect implies that the alloy properties can be greatly adjusted by the composition change and alloying, as shown in Fig. 4, which indicates that the hardness of HEAs can be dramatically changed by adjusting the Al content in the CoCrCuNiAlx HEAs. With the increase of the Al content, the phases change from FCC to BCC + FCC and then to BCC structures. As a result, the lattice constants for both the BCC and FCC structures increase, and the hardness of the alloys increases. Fig. 5. presents the change of hardness as a function of the Al content for the Cu-free CoCrFeNiAlx HEAs. The hardness of the FCC phase does not vary too much with changing the Al content from 0 to 0.45, while the hardness of the BCC phase decreases from about HV 538 to HV 480 as the Al content increases from 0.88 to 2.0. Moreover, the two phase region of FCC + BCC structures becomes much narrower for CoCrFeNiAlx than CoCrCuFeNiAlx indicating that Cu stabilizes the FCC phase. But caution should be addressed here for Cu: Cu tends to segregate and form very Cu-rich phase(s) in CoCrCuFeNiAlx. Cu forms isomorphous solid solution with Ni but it is insoluble in Co, Cr and Fe; it dissolves about 20 at.% Al but also forms various stable intermetallic compounds with Al.

Fig. 6 exhibits the hardness of some reported HEAs in the descending order with stainless steels as benchmark. The MoTiVFeNiZrCoCr alloy has a very high value of hardness of over 800 HV while CoCrFeNiCu is very soft with a value of less than 200 HV. Fig. 7 compares the specific strength, which is defined by the yield strength over the density of the materials, and the density among HEAs, BMGs, conventional alloys, polymers and foam materials.We can see that HEAs

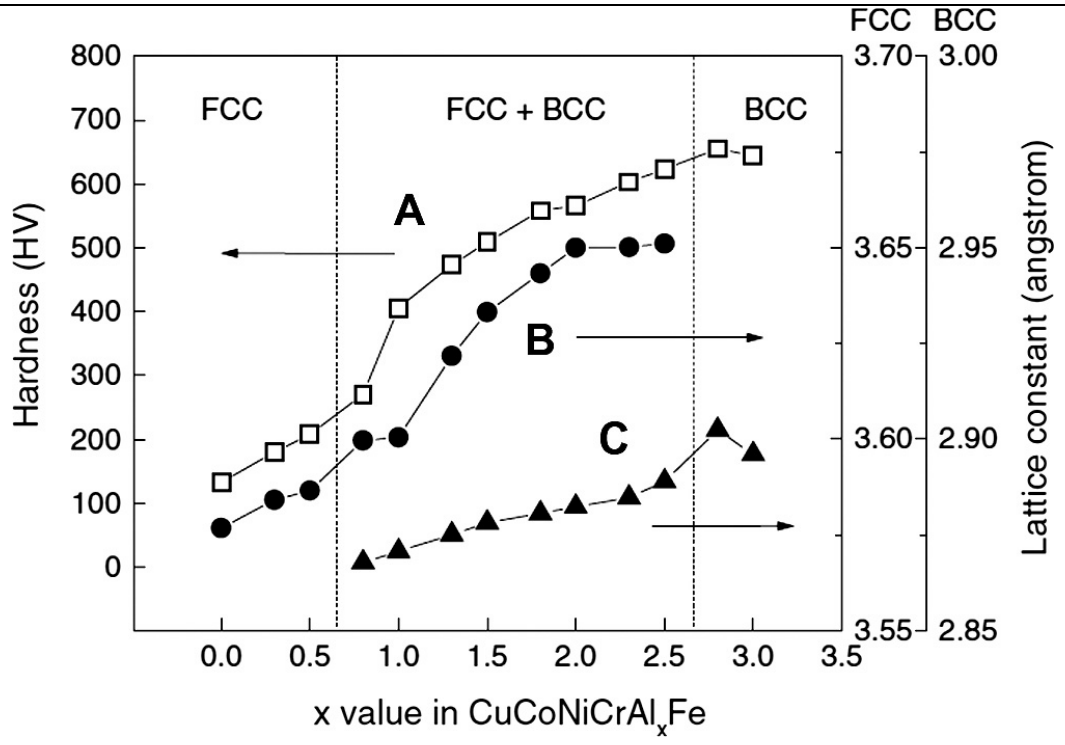

Fig. 4. Hardness and lattice constants of a CuCoNiCrAl$_x$Fe alloy system with different x values: (A) hardness of CuCoNiCrAl$_x$Fe alloys, (B) lattice constants of an FCC phase, (C) lattice constants of a BCC phase.

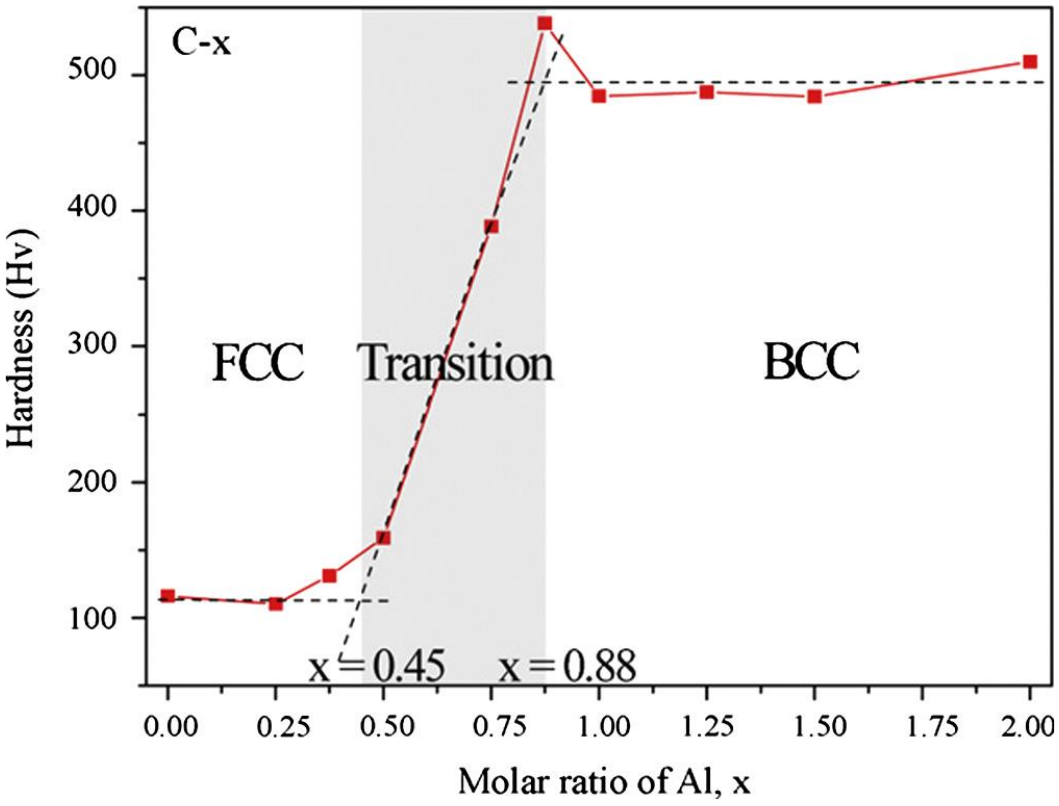

Fig. 5. Hardness of a CoNiCrAl$_x$Fe alloy system with different x values, the Cu-free alloy has lower hardness than that of the CuCoCrAl$_x$Fe alloy.

have densities close to the steel but have high values of specific strength (yield strength/density). This is partially because our recently-reported HEAs usually contain mainly the late transitional elements whose density is on the high side. The lightweight HEAs have much more potential because lightweight elements can be used and the density of the resultant alloys will be lowered significantly. Fig. 8 shows the specific-yield strength of HEAs vs. Young's modulus compared with conventional alloys. As can be seen, HEAs exhibit the highest specific strength and their Young's modulus can be varied in a very large range. This observation may indicate that the modulus of HEAs can be more easily adjusted than conventional alloys. In addition to the high specific strength, other properties such as high hydrogen storage property are also reported.

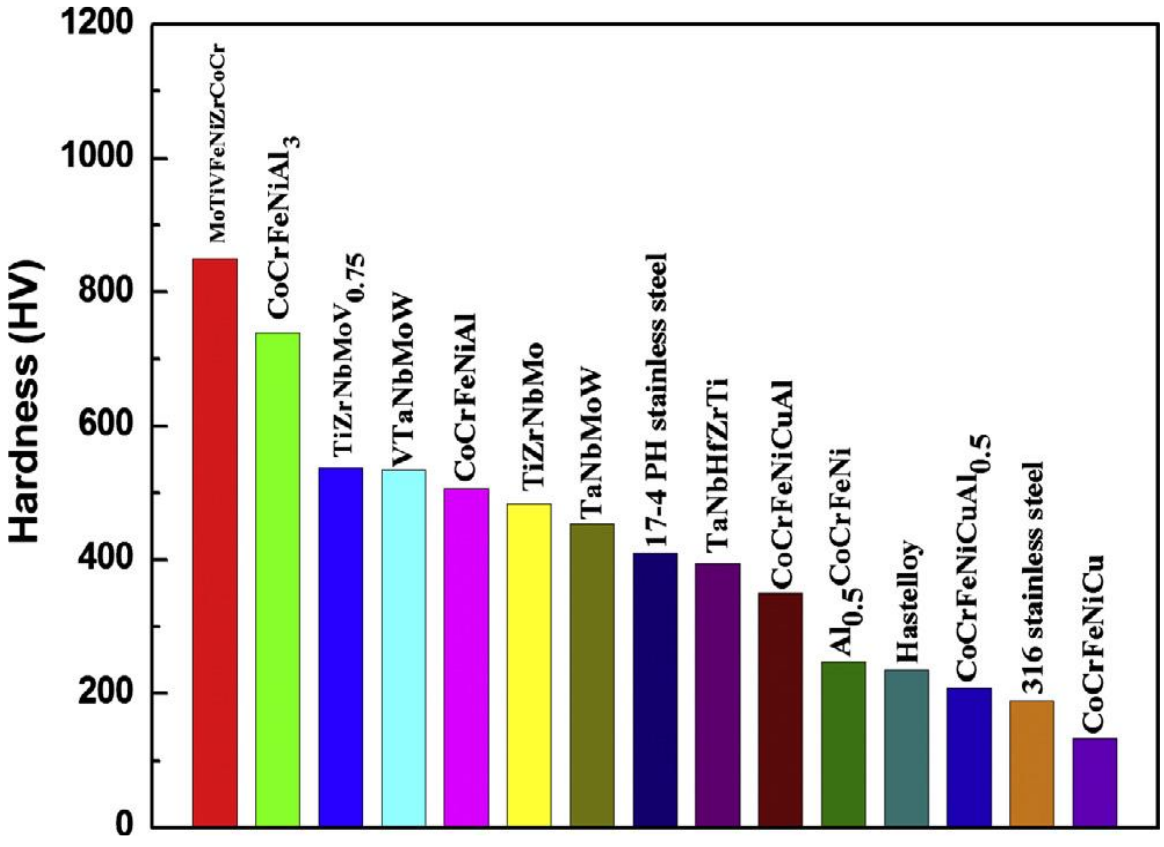

Fig. 6. Wide range of hardness for HEAs, compared with 17–4 PH stainless steel, Hastelloy, and 316 stainless steel.

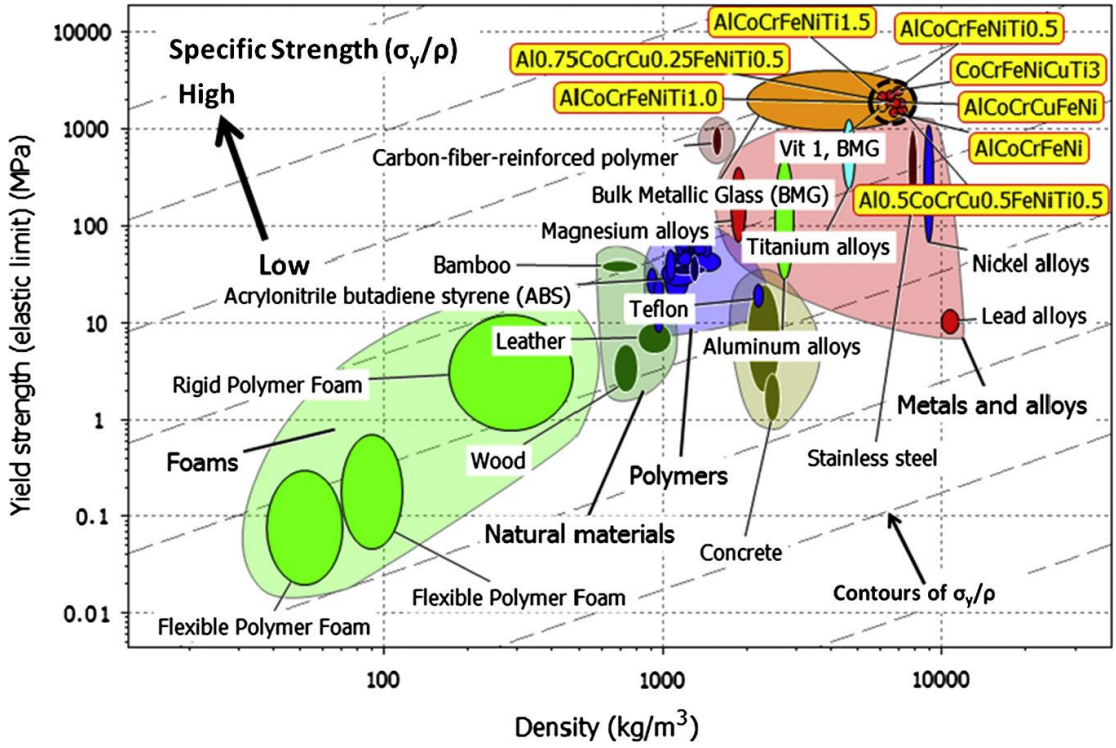

Fig. 7. Yield strength, σ_y, vs. density, ρ. HEAs (dark dashed circle) compared with other materials, particularly structural alloys. Grey dashed contours (arrow indication) label the specific strength, σ_y/ρ, from low (right bottom) to high (left top). HEAs are among the materials with highest strength and specific strength.

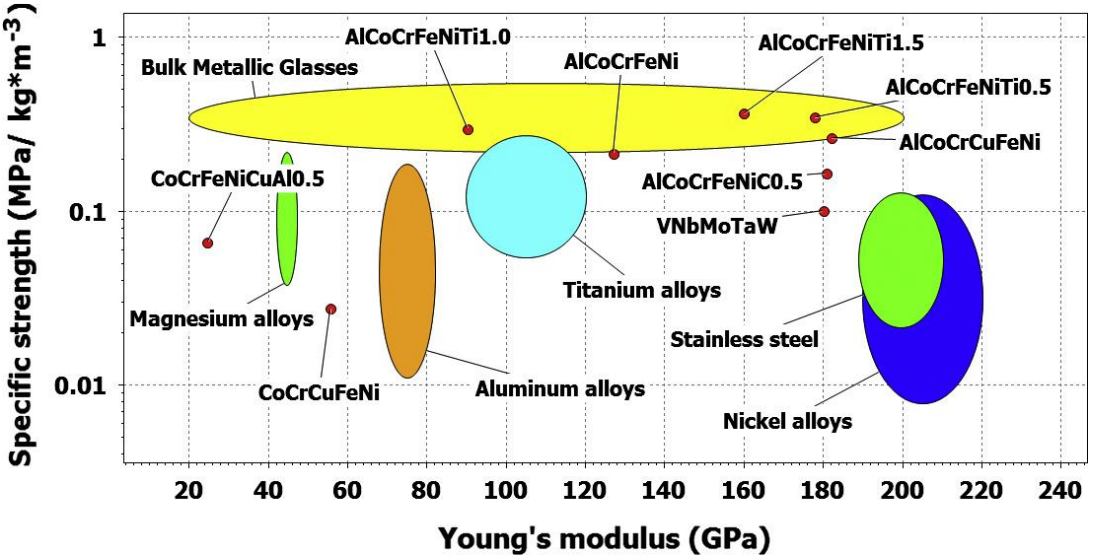

Fig. 8. Specific-yield strength vs. Young's modulus: HEAs compared with other materials, particularly structural alloys. HEAs are among the materials with highest specific strength and with a wide range of Young's modulus.

SECTION III
MICROSTRUCTURE AND MECHANICAL BEHAVIOR OF QUATERNARY HIGH-ENTROPY ALLOY

Microstructure and mechanical behavior of quaternary High-Entropy Alloy

In order to improve the specific strength of the HEAs, the quaternary AlCoCrNi HEA is designed by modulating the alloy component from the AlCoCrFeNi HEA that consists of the Al-Ni-rich B2 matrix with the Cr-Fe-rich A2 nano-particles. In the case of the AlCoCrNi HEA, the atomic ratio of the (Al-Ni)/Cr-Fe) is different compared with the AlCoCrFeNi HEA (1:1 for AlCoCrFeNi, 2:1 for AlCoCrNi), which also gives an opportunity for a decrease of density and the microstructural evolution of the HEAs. Here, the microstructural and chemical features of the AlCoCrNi HEA were systematically investigated to understand its mechanical/physical properties. In addition, the specific yield strength (SYS) at a room temperature and the temperature dependence of hardness of the AlCoCrNi HEA will be discussed through comparing with that of the previous HEAs and a conventional superalloy to evaluate its applicability for engineering materials.

3.1. Experimental procedures

The master ingots of quaternary equi-atomic $Al_{25}Co_{25}Cr_{25}Ni_{25}$ HEA were fabricated using an arc melting with high purity Al, Co, Co and Ni elements of 99.95 at.% under a high purity Ar gas atmosphere (99.99%). The ingots were remelted at least five times to ensure chemical homogeneity. As-cast rod samples were prepared using suction casting into a cylindrical rod-shaped copper mold with diameters of 3mm and 50mm in length. The phase identification of the as-cast sample was performed using X-ray diffraction (XRD, D2 phaser, Bruker) with Co Kα radiation (λ═1.79026 Å) and transmission electron microscopy (TEM, Tecnai-F20) with energy dispersive spectrometry (EDS). Thin film specimens for TEM analysis were prepared by ion milling with liquid nitrogen cooling. The cross-sectional microstructure of the as-cast sample was investigated by scanning electron microscopy (SEM, JEOL JSM-6390; JEOL) with energy-dispersive spectrometry. The volume fraction of constituent phases in the as-cast sample was estimated using

a pixel analysis of the SEM micrographs obtained from the cross-sectional area and the TEM high-angle annular dark field (HAADF) images of the as-cast sample. The mechanical properties of the as-cast sample were examined by a compression test at a strain rate of 1 x $10^{-3}s^{-1}$ using the cylindrical sample with a 2:1 aspect ratio. Nanoindentation experiments were performed to measure the hardness of the as-cast sample in a load-control mode conducted with a maximum load of 25mNat a constant loading/unloading rates of 15 mNs^{-1} using a nano-indentation tester (CSM NHT-X). Rockwell C hardness test was also conducted using a 120-degree diamond indenter under 1471 N load at temperatures ranging from 293 to 973 K. The density of the as-cast sample was measured via hydrostatic
weighing.

3.2. Results and discussion

Crystal structures of the as-cast AlCoCrNi HEA were determined from the XRD pattern shown in Fig. 1(a). In order to identify clearly the XRD pattern obtained using Co Ka radiation, the contribution of Ka2 radiation is stripped using the software. The as-cast alloy exhibits the diffraction patterns of the disordered A2-bcc phase with the ordered B2-bcc phase and clearly shows the (100) plane of the B2 phase. The microstructural features, i.e., the formation of the A2/B2 dual-phase structure, have also been identified in the AlCo-FeCrNi HEA. The cross-sectional SEM backscattered electron (BSE) micrograph of the as-cast AlCoCrNi HEA in Fig. 1(b) reveals a typical microstructure of dual-phase HEAs consisting of DR (dark) and ID (bright) regions. The volume fraction of the DR and ID is estimated as 59.6 ± 2.1% and 40.4 ± 2.1%, respectively. The chemical composition of both regions measured by EDS is listed in Table 1. The DR region exhibits a higher concentration of the Al and Ni and a lower amount of Cr than the ID region, which indicates that the solute segregation into the Ni-Al-rich and Cr-rich regions occurred during the dendritic solidification. The segregation of the Cr content
during the solidification has also been reported in previous studies on AlCoCrFeNi HEA. Based on these results in Fig. 1, it is confirmed that the AlCoCrNi HEA designed by excluding the Fe content from the AlCoCrFeNi HEA solidifies into

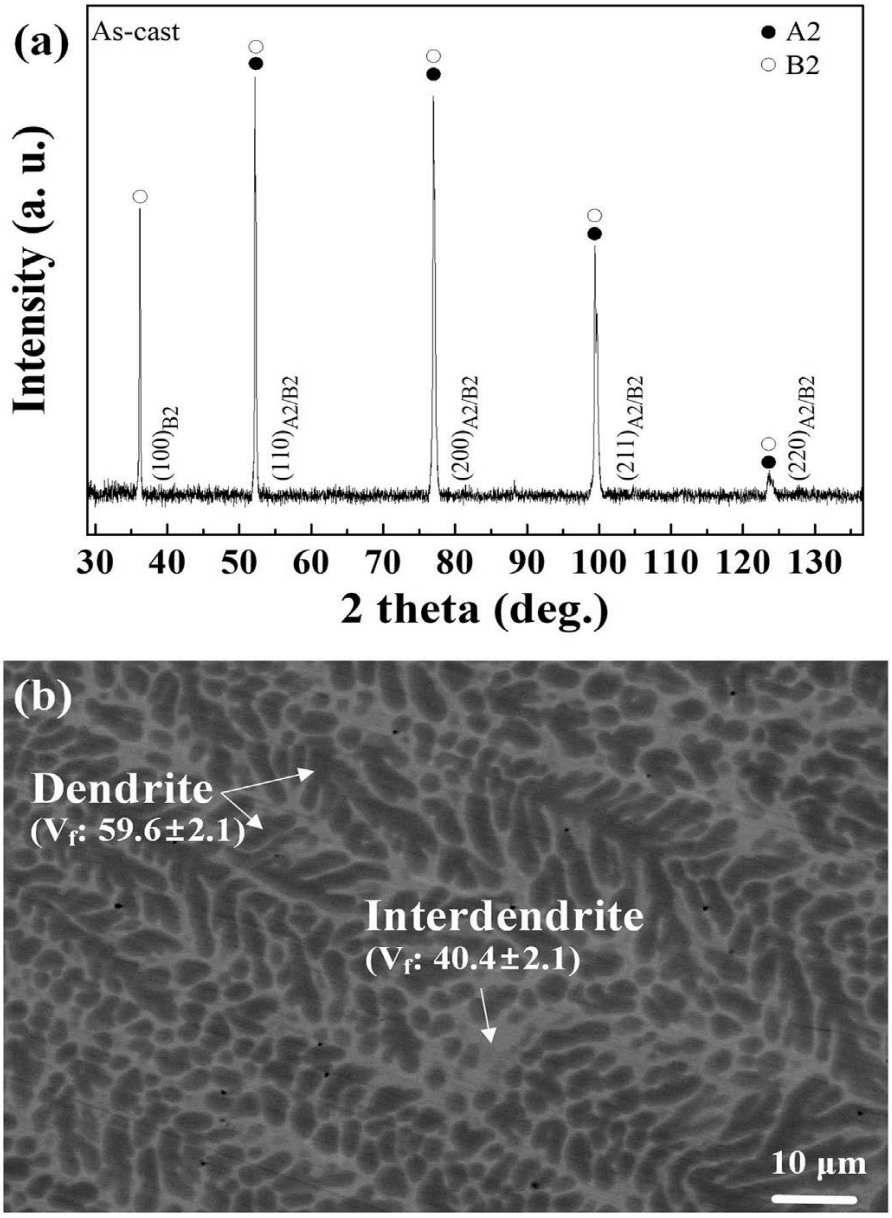

Fig. 1. (a) XRD pattern and (b) SEM BSE micrograph of as-cast AlCoCrNi alloy.

Table 1

Chemical composition of the dendritic and the interdendritic regions of the as-cast AlCoCrNi alloy.

Region	Al (at.%)	Co (at.%)	Cr (at.%)	Ni (at.%)
Dendrite	28.4	25.3	16.0	30.3
Interdendrite	18.4	26.7	31.7	23.2

the Ni-Alrich DR and Cr-rich ID regions that consisted of the A2/B2 dualphase structure, which is very similar to the microstructural morphologies of the AlCoCrFeNi HEA.

In order to obtain a profound insight into the microstructural characterization of the as-cast AlCoCrNi HEA, the TEM analysis was performed. Fig. 2 illustrates

the HAADF scanning transmission electron microscopy (STEM) images, the selected area electron diffraction (SAED) patterns, the EDS elemental maps, a high-resolution transmission electron microscopy (HRTEM) image and the fast Fourier transform (FFT) with corresponding inverse FFT dark field (DF) image obtained from the as-cast AlCoCrNi HEA. The HAADF image in Fig. 2(a) exhibits the dark contrasted DR region embedded in the bright contrasted ID region as a result of the dendritic solidification. Fig. 2(b) displays the SAED pattern recorded along the zone axis of the bcc phase from the DR area, clearly indicating the diffraction spots corresponding to the A2 phase as well as the superlattice of the B2 phase. For the ID region, the SAED pattern in Fig. 2(c) also shows the diffraction spots of zone axis corresponding to the A2 phase with a superlattice of the B2 phase. These results indicate that both DR and ID regions consist of the disordered A2-bcc and the ordered B2-bcc phases. Fig. 2(d) exhibits the magnified HAADF image obtained from the boundary area between the DR and the ID regions in Fig. 2(a), and the regional boundary is marked by a white dotted line. As a result of the SAED patterns, the dual-phase structure in both DR and ID regions are confirmed as shown in Fig. 2(d). The elemental distributions of Al, Ni, Cr, and Co in both the DR and the IR regions are measured using EDS elemental maps. Fig. 2(e) shows the STEM HAADF image (left) of the DR region and corresponding EDS elemental maps (right) for Al, Ni, Cr and Co elements. The Al and Ni content are concentrated in a dark contrasted phase, whereas the Cr content is strongly concentrated in a bright contrasted particle phase. Meanwhile, the Co content is dispersed similarly in both phases. Fig. 2(f) exhibits the STEM HAADF image (left) of the ID region and corresponding EDS elemental maps (right). Similarly with the DR region, the high level of Al and Ni concentration is also detected in the dark contrasted phase and the Cr is concentrated on the bright contrasted phase. In the DR region, the Co content also is dispersed similarly in both phases. In order to obtain the quantitative chemical composition of the dark and bright phases in both regions, the EDS analysis was performed, and the results are listed in Table 2. From the SAED patterns and the EDS results, it is confirmed that the DR and the ID regions consist of the same phases, revealing that the bright and dark contrasted phases in both

regions are the Cr-rich A2 phase and the Ni(Co)-Al-rich B2 phase, respectively. The crystal structure of both Cr-rich A2 and Ni(Co)-Al-rich B2 phases is also confirmed by HRTEM analysis. Fig. 2(g) displays the HRTEM image obtained from the white dotted rectangle area in Fig. 2(d) and the FFT patterns corresponding to the i) and the ii) areas are shown in Fig. 2(h) and (i), respectively. The FFT pattern taken from the i) area in Fig. 2(g) shows the diffraction spots of the zone axis of the A2 phase [see Fig. 2(h)], whereas the ii) area reveals the zone axis of the B2 structure with the distinct superlattice shown in Fig. 2(i). The DF image taken from the additional spots [marked by an arrow in Fig. 2(i)] is shown in Fig. 2(j). It can be immediately seen that the ID region consists of the A2/B2 dual-phase structure without any other phase.

On the one hand, the ID region in Fig. 2(d) is characterized by an intertwined structure consisted of the Ni(Co)-Al-rich B2 precipitates and the Cr-rich A2 matrix where both phases alternate with an inter-phase spacing of ~50 nm. On the contrary, the DR region exhibits an inverted microstructural morphology where the highly dense Cr-rich A2 precipitates of the cuboidal morphology with a length of ~50 nm formed in the Ni(Co)-Al-rich B2 matrix. The inverted microstructures between the ID and the DR regions can be considered as a result of the segregation of a large amount of Cr content into the ID region during the dendritic solidification. The volume fraction of the DR/ID regions and the A2/B2 phases in both regions are estimated and summarized in Table 3. The measured total volume fraction of the Cr-rich A2 and the Ni(Co)-Al-rich B2 phases in the AlCoCrNi HEA is about 44.9 ± 2.1% and 55.1 ± 2.1%, respectively. These microstructural features of the AlCoCrNi HEA are quite different compared with the AlCoCrFeNi HEA. In the case of the previously reported AlCoCrFeNi HEA, the Cr-Fe-rich A2 phase was usually precipitated in the Ni-Al-rich B2 matrix in both the DR and the ID regions even if the total volume fraction of the Cr-Fe-rich A2 phase (52 vol%) is higher than the Ni-Al-rich B2 phase (48 vol%). Furthermore, the Ni-Al-rich B2 phase ($Al_{30.3}Co_{20.2}Cr_{5.2}Fe_{13.9}Ni_{30.4}$ in at.%) in the AlCoCrFeNi HEA consisted of the equi-atomic ratio for Ni and Al. On the other hand, the Ni(Co)-Al-rich B2 phase in the AlCoCrNi HEA contains a relatively higher content of Ni (about 38 at.%) than Al

content (about 22 at.%). Previous studies have reported the composition dependence of micro-hardness for the Ni-Al B2 intermediate alloys, and it will be discussed in Fig. 3. Therefore, the formation of the Ni(Co)-Al-rich B2 phase with a high amount of Ni, as well as a higher volume fraction than the Cr-rich A2 phase in the AlCoCrNi HEA can give an opportunity to enhance the mechanical properties and a specific strength of the dual-phase HEAs.

The mechanical properties of the as-cast AlCoCrNi HEA at room temperature were determined by the compression and the nanoindentation tests. Fig. 3(a) shows the compressive stress-strain curve of the as-cast AlCoCrNi HEA, in conjunction with an inset typical load-displacement curve of the nano-indentation. The yield strength, maximum compressive strength, plasticity and indentation hardness of the

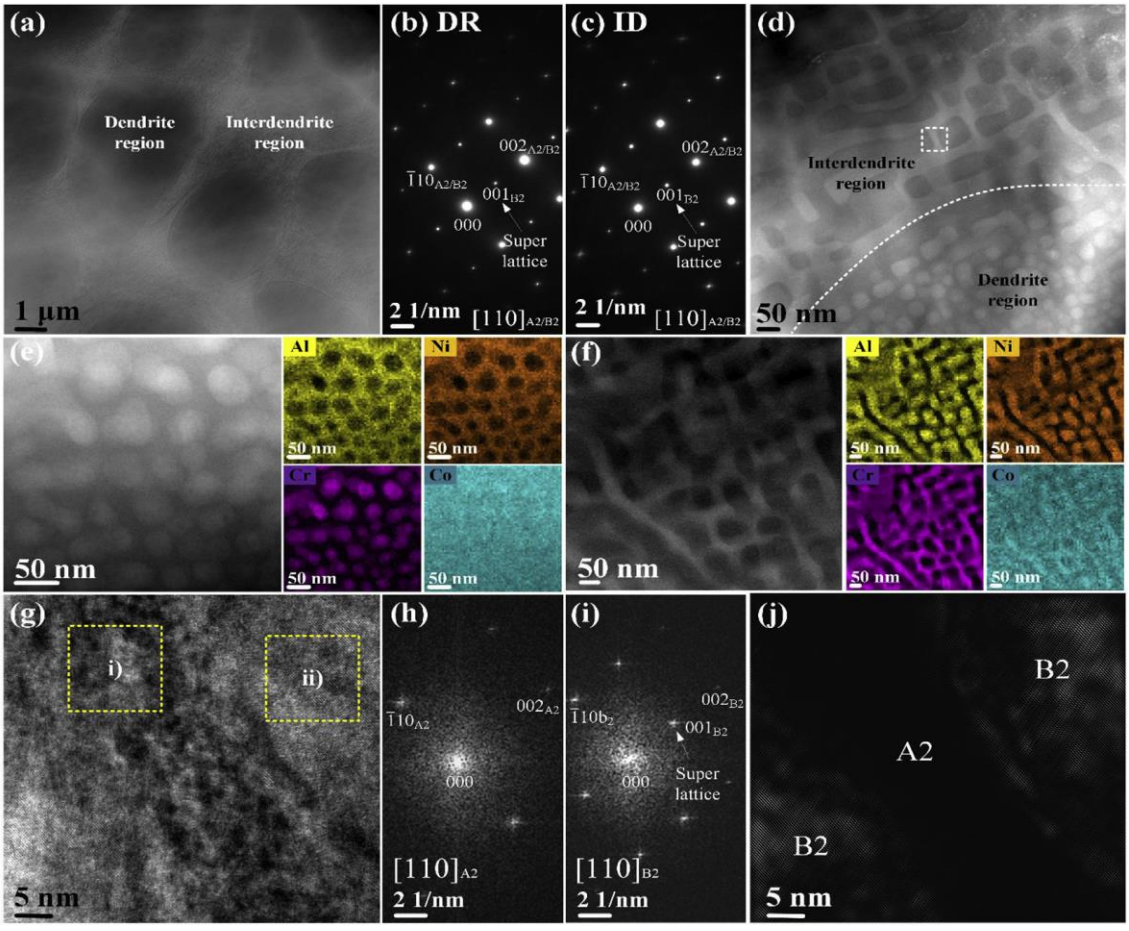

Fig. 2. [(a) and (d)] STEM HAADF images and [(b) and (c)] SAED patterns correspond dendritic and interdendritic regions, [(e) and (f)] STEM HAADF images with corresponding EDS elemental maps taken from the dendritic and interdendritic regions, (g) HRTEM image obtained from the white dotted rectangle in Fig. 2(d), [(h) and (i)] FFT patterns taken from i) and ii) areas in Fig. 2(g) and (j) corresponding DF image of as-cast AlCoCrNi alloy.

Table 2

Chemical composition of the nano-scale A2 and B2 phases in both the dendritic and interdendritic regions of the as-cast AlCoCrNi alloy measured by TEM EDS analysis.

Region	Phase	Al (at.%)	Co (at.%)	Cr (at.%)	Ni (at.%)

Dendrite	A2	8.9	28.8	48.2	14.1
	B2	23.2	28.3	9.2	39.3
Interdendrite	A2	3.1	30.7	60.6	5.6
	B2	20.3	27.3	15.2	37.3

Table 3
Volume fraction of micro-scale dendritic and interdendritic regions estimated from SEM analysis and volume fraction of nano-scale A2 and B2 phases in both the dendritic and the interdendritic regions estimated from the TEM analyses.

Region	Vol%	Phase	Vol%
Dendrite	59.6	A2	24.1
		B2	35.5
Interdendrite	40.4	A2	20.8
		B2	19.6

as-cast AlCoCrNi HEA and the previous AlCoCrFeNi HEA are summarized in Table 4. The AlCoCrNi HEA exhibits a remarkably improved yield strength without a trade-off between the strength and plasticity compared with AlCoCrFeNi HEA. In order to identify the origin of the strengthening on the as-cast AlCoCrNi HEA, the nano-indentation was performed as shown in the inset curve in Fig. 3(a). The indentation hardness (HIT) of the as-cast AlCoCrNi HEA is about ~11.6 GPa on both the ID and the DR regions, which is higher than that of AlCoCrFeNi HEA (~9.86 GPa). As mentioned above the TEM and the EDS results in Fig. 2, even though the AlCoCrNi HEA consists of the nano-scale A2/B2-bcc phases that are similar to the AlCoCrFeNi HEA, there are significant differences in the chemical compositions. Whereas the Ni-Al-rich B2 phase in the previous AlCoCrFeNi HEA has exhibited a stoichiometric composition between the Ni and the Al content, the Ni(Co)-Al-rich B2 phase in the AlCoCrNi HEA has a non-stoichiometric composition between the Ni and the Al content. It is known that the composition dependence of the micro-hardness of the NixAl100-x (x j 46 to 60 at.%) intermediate phase in ultrafine-grained as well as coarse-grained NiAl alloys.

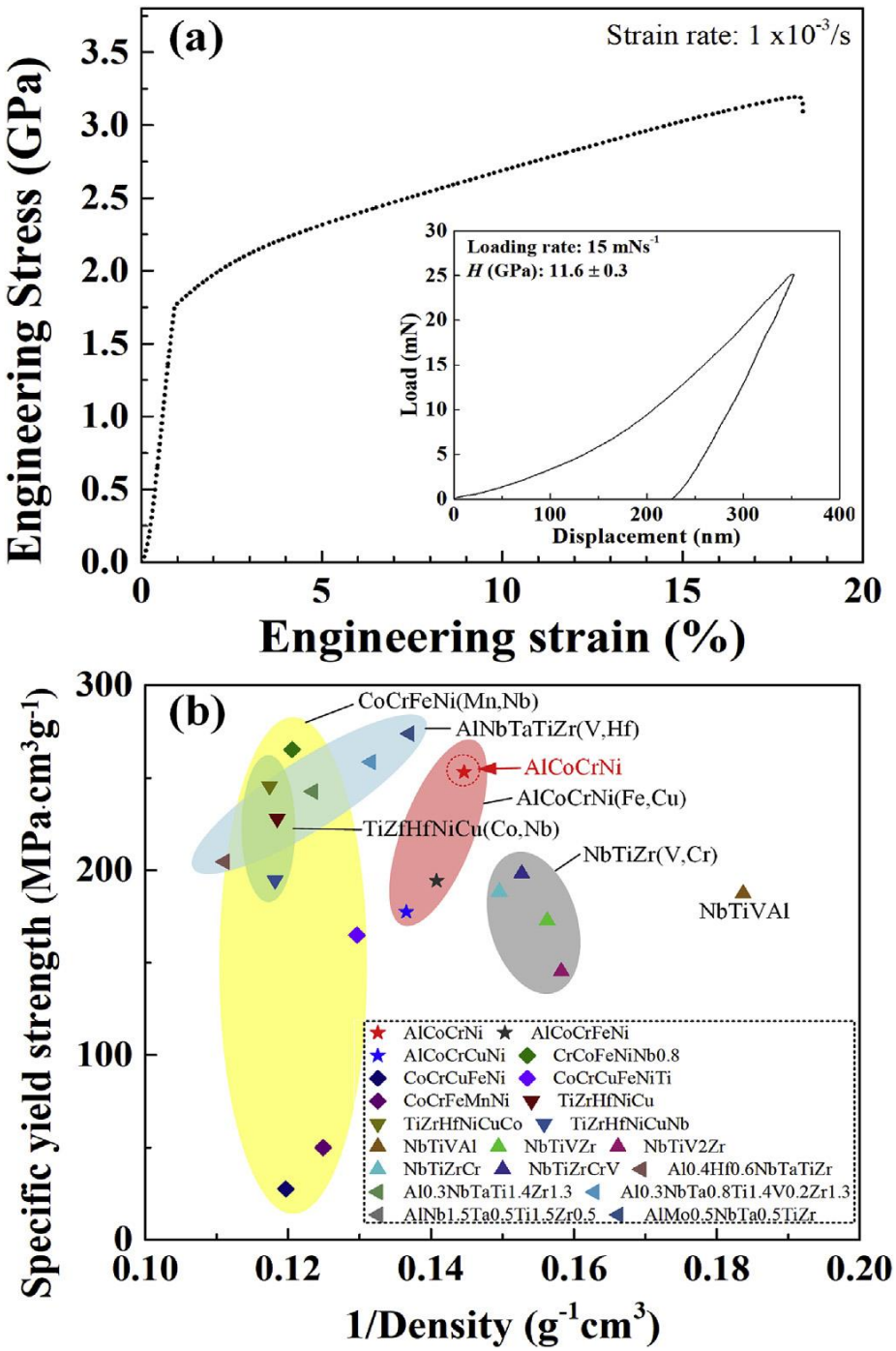

Fig. 3. (a) Compressive stress-strain curve of as-cast AlCoCrNi alloy with inset loaddisplacement curve of nano-indentation and (b) comparison of specific yield strength vs 1/density between as-cast AlCoCrNi alloy with previous reported HEAs.

When the atomic ratio of the Ni and the Al within the B2 phase field deviates from the stoichiometric composition (1:1), the micro-hardness of the Ni-Al B2 phase significantly increases with an increasing atomic-level strain. Therefore, it is believed that the formation of the Ni(Co)-Al-rich B2 intermediate phase with a non-stoichiometric composition between the Ni and Al content (see Table 2) and the

increasing volume fraction of the phase effect the enhancement of the mechanical properties of the AlCoCrNi HEA.

Based on this result, an SYS and the density of as-cast AlCoCrNi alloy are compared with previous HEAs. As illustrated in Fig. 3(b), the Al-containing AlNbTaTiZr(Mo,V,Hf) dualphase HEAs exhibit a superior SYS above 250 MPa cm^3g^{-1} at room temperature compared to the Al-free NbTiZr(V,Cr) singlephase HEA. However, the AlNbTaTiZr(Mo,V,Hf) HEAs with superior SYS usually reveal the limited macroscopic plasticity, which limits their structural application. On the other hand, the AlCoCrNi HEA with the macroscopic plasticity exhibits not only lower density (~6.9 gcm^{-3}) but also high SYS (above 250 MPa cm^3g^{-1}) compared with the AlNbTaTiZr(V,Hf) and the AlCoCr(Fe,Cu)Ni dual-phase HEA systems, which results from the increasing lightweight Al content and the removing of heavy element, such as Fe.

The temperature dependence of mechanical properties of the as-cast AlCoCrNi HEA was investigated by performing Rockwell C hardness tests at various temperatures. In addition, the Inconel 713C Ni-based superalloy (as-received), which are well-known as high-temperature structural materials, was also tested. Fig. 4 shows Rockwell C hardness values of the as-cast AlCoCrNi HEA and the Inconel 713C alloys at temperatures ranging from 298 to 973 K. The as-cast AlCoCrNi HEA exhibits much higher hardness values than that of the Inconel 713C superalloy, which is well maintained without a significant decrease of hardness to 873 K. It is well known that the Al-containing dual-phase HEAs that consist of the bcc phases with a high degree of coherence usually show superior strength at a high temperature due to the fully isolated dual-phase structure and its high-temperature phase stability. The AlCoCrNi HEA also consists of the nano-scale A2/B2-bcc dual-phase structure with the high degree of coherence as demonstrated on the TEM results in Fig. 2. Moreover, the attractive hardness values of the as-cast AlCoCrNi HEA at a high temperature is also higher than that of other Al-containing dual-phase HEAs, which is attributed to the highly enhanced mechanical properties at room temperature by the chemical and microstructural evolutions in the AlCoCrNi HEA. From the investigations on the microstructure and the mechanical properties of the

as-cast AlCoCrNi HEA, it is suggested that the modest changes on the chemical composition of the constituent phases with preserving the crystal structures and high degree of coherence can strongly influence the mechanical properties of the Al-containing dual-phase HEAs, which can be considered as a way to improve the mechanical properties of the nano-scale dual- or multi-phase HEAs.

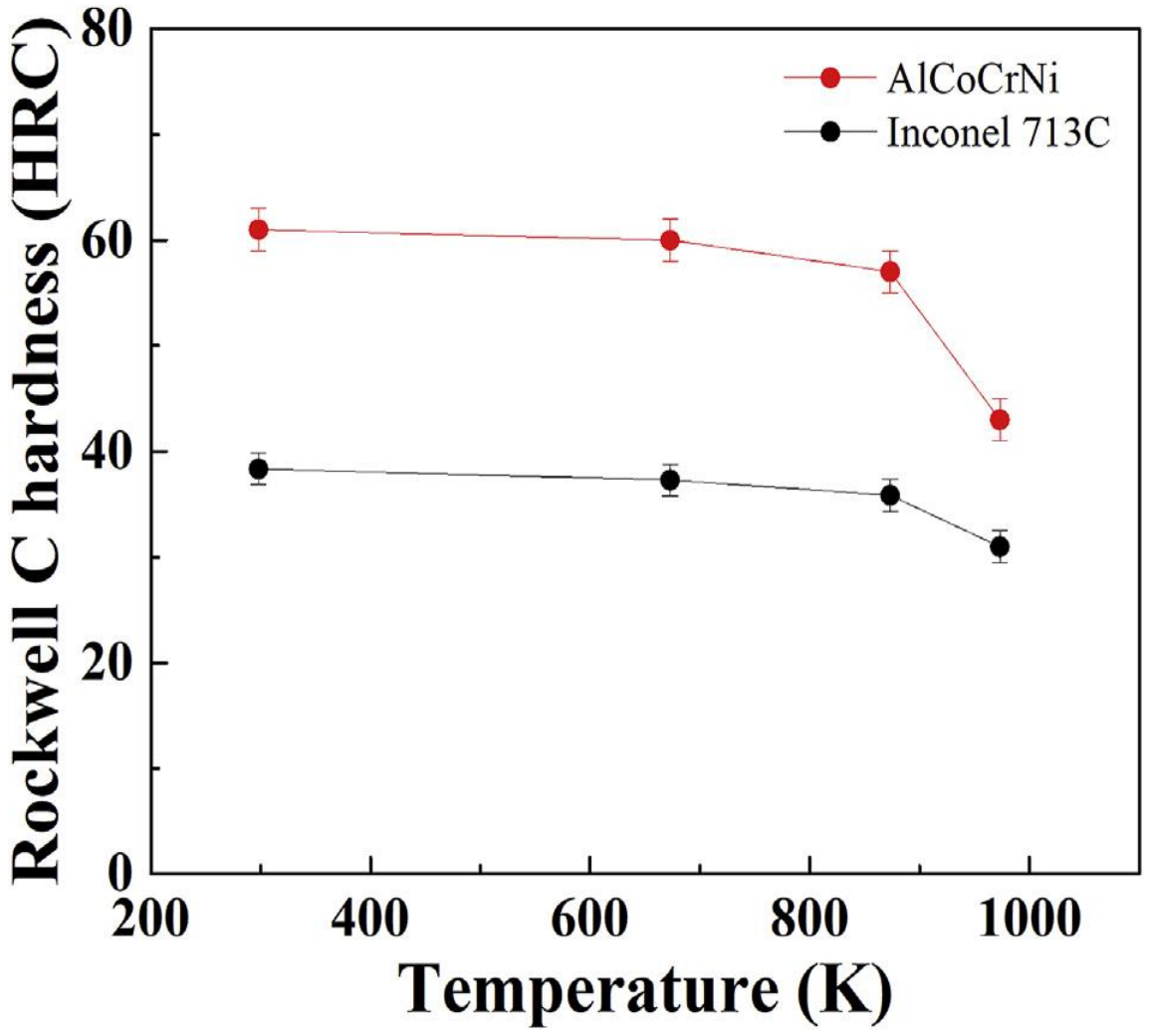

Fig. 4. Comparison of Rockwell C hardness values of as-cast AlCoCrNi and Inconel 713 alloys at temperatures ranging from 293 to 973 K.

Table 4
Yield strength (σ_y), maximum strength (σ_{max}), plasticity (ε_p) and indentation hardness (H_{IT}) of the as-cast AlCoCrNi alloy determined by compression and nano-indentation tests.

Alloy	σ_y (MPa)	σ_{max} (MPa)	ε_p (%)	H_{IT} (GPa)
AlCoCrNi [present]	1750 ± 50	3200 ± 35	16.7 ± 0.9	11.6 ± 0.2 (at 15 mNs¯1)
AlCoCrFeNi	1384	1912	16.7	9.86 at (at 10 mNs¯1)

SECTION IV

EFFECTS OF MN AND V ON MICROSTRUCTURE AND MECHANICALPROPERTIES OF HIGH-ENTROPY ALLOYS BASED ON ALCOCRNI SYSTEM

Effects of Mn and V on microstructure and mechanicalproperties of high-entropy alloys based on AlCoCrNi system

The concept of high entropy alloys (HEAs) is one of the most recent developments in material science. Depending on their composition and microstructure, HEAs can offer diverse range of attractive properties, such as high hardness and wear resistance, exceptional high temperature strength, good low-temperature ductility, and superplastic behavior. High entropy of mixing is thought to prevent formation of intermetallic phases. Thus, the alloys should consist mainly from simple solid solutions. However, there are experimental evidences that ordered solid solutions and intermetallic phases may also exist in many HEAs. This indicates that the high entropy of mixing of the alloying elements is not sufficient to prevent formation of intermetallic phases in favorof solid solution phases in HEAs.

It is known that several 4-component equiatomic alloys, such as WNbMoTa or AlCoCrNi exhibit simple solid solution single phase structures. Increasing the number of alloying elements generally causes phase separation, in spite of an increase in ΔS_{mix}. For example, a complex multiphase structure is formed in the AlCoCrNi system. In contrast, in the AlCoCrNiMn alloy the presence of only simple solid solution is confirmed by anumber of investigations. Such different behavior can be expected, as Mn is closer to the other components ofthe alloy to fulfill Hume-Rothery rules. Another ‘‘neighbor’’ of the elements of the AlCoCrNi alloy in the periodic table is V. I did not find any information in the literature on the alloys with compositions close to AlCoCrNiV and AlCoCrNiMnV. But, complex structures containing intermetallic phases, including the σ phase, were reported for the $Al_{0.5}CoCrCuFeNiV_x$ alloy system. The σ phase was also found in the alloy AlCoCrNiMnV. However, the presence of such element as Al and Mn or the absence of Cr makes it impossible to clearly denote the effect of V on the microstructure formation of the AlCoCrNi-based alloys.

In this work, the microstructure and mechanical properties of the AlCoCrNi, AlCoCrNiMn, AlCoCrNiV and AlCoCrNiMnV HEAs are reported, both in as-

solidified condition. Mn and V were chosen as the alloying elements as they are ‘‘neighbors’’of the elements of the base alloy in the periodic table and thus are likely to form simple solid solutions. The following goals were pursued: (I) to investigate the effects of alloying with V alone or together with Mn on the microstructure of AlCoCrNi alloy; and (II) to evaluate mechanical properties of the $AlCoCrNiMn_xV_y$ alloys and their interplay with the microstructure.

4.1. Experimental procedures

Equiatomic alloys with the compositions of AlCoCrNi, AlCoCrNiMn, AlCoCrNiV and AlCoCrNiMnV were produced by vacuum arc casting equipment of the components in high-purity argon inside a water-cooled copper cavity. The purities of the alloying elementswere above 99.9%. To ensure chemical homogeneity, the ingots were flipped overand re-melted a least 5 times. The produced ingots had dimensions of about 3 x 10 x 50 mm. The alloys were studied in as-solidified state. Prior to homogenization, the sampleswere sealed in vacuumed (10^{-2} torr) quartz tubes filled with titanium chipsto prevent oxidation.

Microstructure of the alloys was studied using X-ray diffraction (XRD), and scanning (FE-SEM) and transmission (TEM BF) electron microscopy. XRD analysis was performed using RIGAKU diffractometer and Cu Kα radiation. Samples for FE-SEM observations were prepared by careful mechanical polishing. SEM investigations were performed utilizing Quanta 200 3D microscope equipped with energy-dispersive (EDX) detector. Samples for TEM analysis were prepared by conventional twin jet electro-polishing of mechanically pre-thinned to 100 μm foils, in a mixture of 95% C_2H_5OH and 5% $HClO_4$ at the 27 V potential. TEM investigations were performed using JEOL JEM-2100 apparatus equipped with EDX detector at accelerating voltage of 200 kV.

Compression testing was preformed utilizing Zwik 660 UTM machine. Specimens rod type dimensions of 3 x 6 mm. Three compression specimens were tested for each condition.

4.2. Results

As-solidified condition

XRD patterns of the as-solidified alloys are shown in Fig. 1. Thepattern of the base AlCoCrNi alloy demonstrates the presence of a two phase with the BCC lattice. The BCC phase, with a slightly higher lattice parameter is also found in the AlCoCrNiMn alloy. The XRD pattern from this alloy shows only two peaks, BCC and B2 which are an indication of the formation of very large grains in this alloy after solidification. Addition of V both to the base and to the Mn-containing alloys, causes formation of the changes of volume fracture.

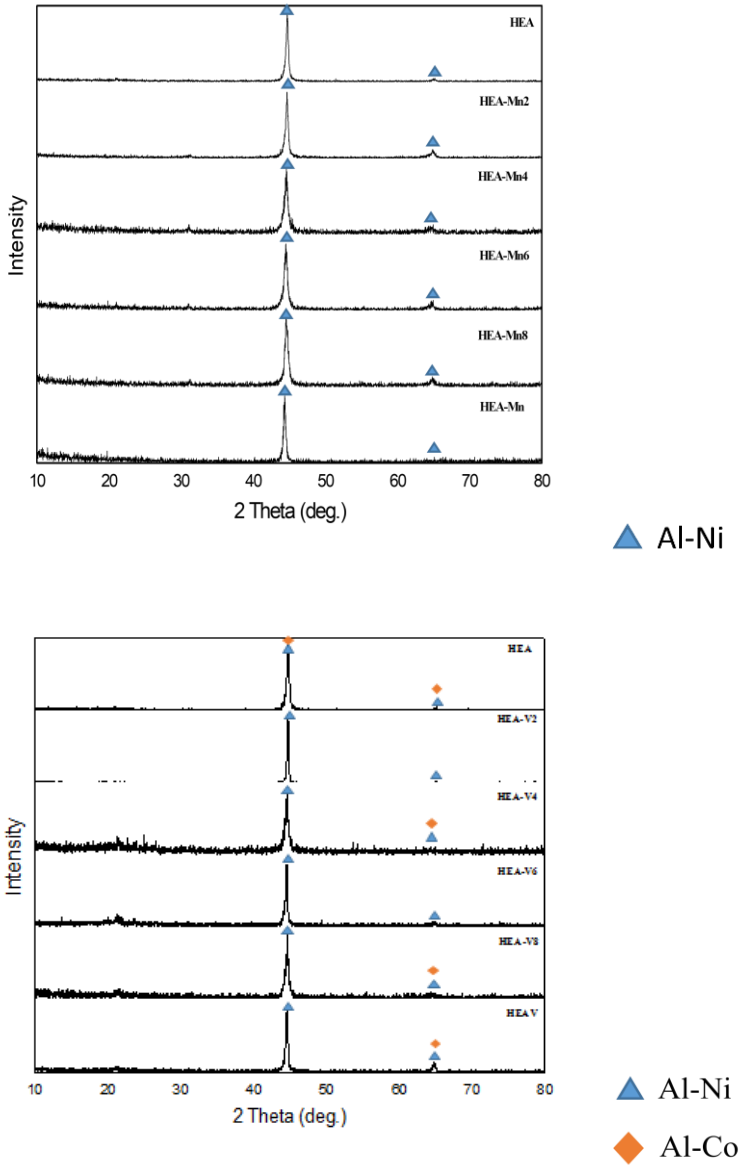

Fig. 1. X-ray diffraction patterns of the studied alloys in as-solidified condition.

The microstructures of the as-solidified alloys are shown in Fig. 2. The base AlCoCrNi alloy has a two phase structure (Fig. 2a). The measured compositions of grains are reasonably close to the nominal composition of the alloy (Table1). The AlCoCrNiMn alloy has a dendritic microstructure (Fig. 2b); the dendrite areas (light-grey ones) are slightly enriched with Co, Cr and Al (Table 1) and contain about 24.5–25% of Ni and Mn. Contrary, inter-dendritic areas (dark-grey ones) are enriched with Ni and Mn and contain about 24–25% of each of the remaining elements. The AlCoCrNiValloy has a complex microstructure (Fig. 2c) composed from grain boundary phase, enriched with Ni and depleted of Cr (Table 1), and grain interiors, slightly enriches with Cr and depleted of Ni. The grain interior consists of two phases with veryfine scale (shown in a higher magnification insert): dark matrixand light elongated particles. This type of microstructure generally occurs after eutectoid transformation. The microstructure of the AlCoCrNiMnV alloy (Fig. 2d) is similar to the AlCoCrNiV alloy. Thegrain boundary phase is enriched with Ni and Mn, and grain interiorsare slightly enriched with Cr and V (Table 1). The difference between the microstructures of the AlCoCrNiV and AlCoCrNiMnV alloys is found inside the grain interiors (shown in a higher magnification insert): the second-phase particles have more equiaxed shape and are coarser in the alloy with Mn.

Additional information about the microstructure of the alloys was obtained from TEM investigations. TEM confirms that the base AlCoCrNi alloy has a two phase BCC crystal structure and all grains have nearly nominal chemical composition (Table 2). At the same time, slight variations of the chemical composition of the BCC phase are found in the AlCoCrNiMn alloy (Table 2); the chemical compositions of the dendrite and interdendrit eareas were determined to be similar to those determined by SEM-EDX. There demonstrate grain interiors of the AlCoCrNiV and AlCoCrNiMnV alloys. Both of them have similar features.The matrix phase has a B2 structure and thus is identifiedas a σ phase. It is enriched with Cr and V, and depleted of Ni (and Mn in the alloy containing Mn). Inside the matrix, elongated particles with the BCC structure are found. These particles are

depleted of Cr and V and enriched with Ni (and also Mn, in the alloy containing Mn).

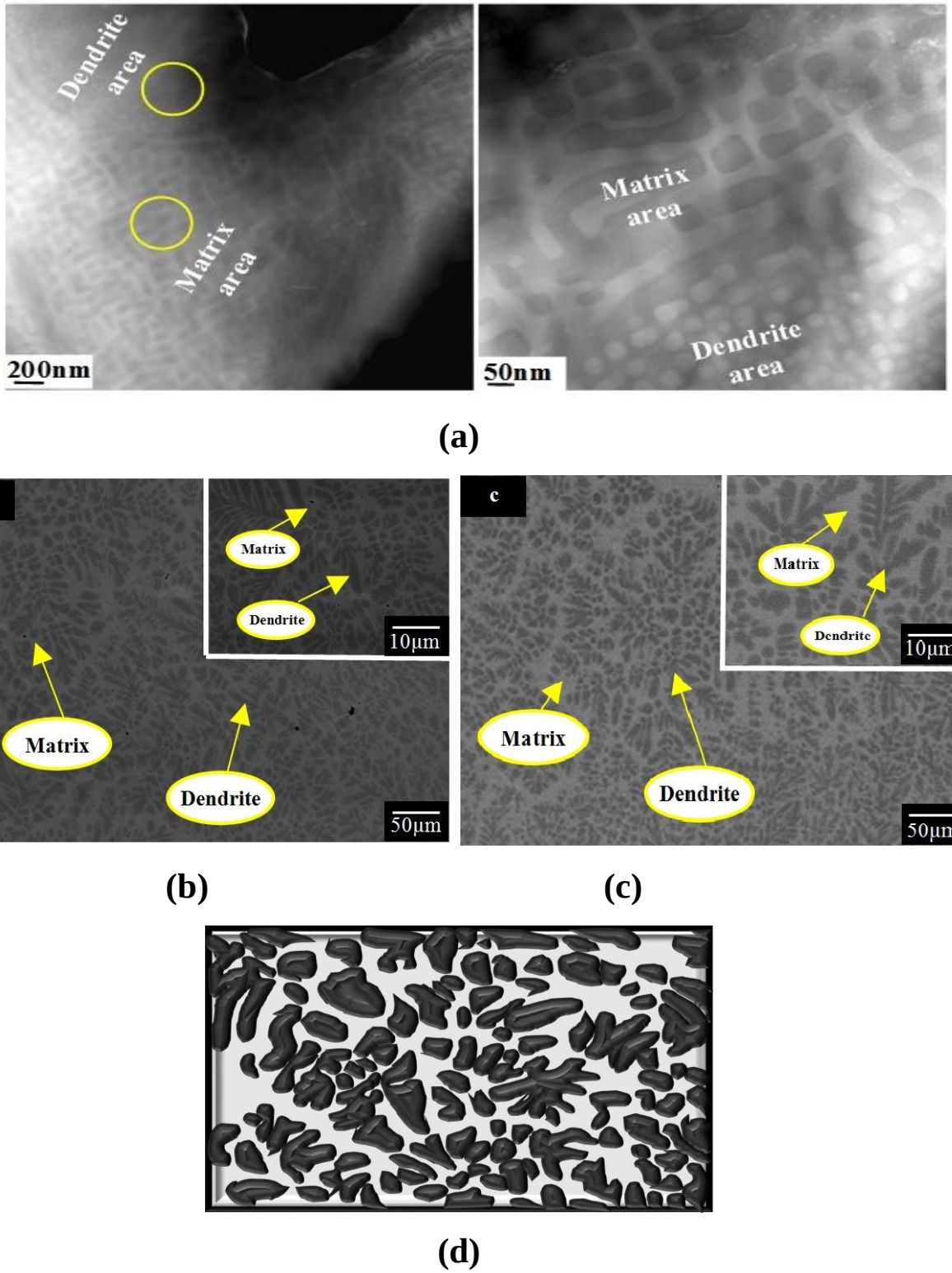

Fig. 2. Backscatter electron (BSE) images of the microstructure of the studied alloys in the as-solidified condition: a) AlCoCrNi, (b) AlCoCrNiMn, (c) AlCoCrNiV, and (d) AlCoCrNiMnV. Different structural constituents are dentified with numbers and their compositions are given in Table 1.

Table 1

Chemical composition of the alloy constituents (as shown in Fig. 2) in the as-solidified condition. The data derived by SEM-based EDX.

Element, at.%	Al	Co	Cr	Ni	Mn	V
AlCoCrNi						
1. Grains	25.2	24.7	25.3	24.8	-	-
AlCoCrNiMn						
1. Dendrites	22.1	21.0	21.8	16.7	16.4	-
2. Interdendrites	16.7	16.8	17.0	22.9	26.6	-
AlCoCrNiV						
1. Grain boundary phase	19.4	20.9	17.0	24.4	-	18.3
2. Grain interiors	20.0	18.9	22.1	17.8	-	21.2
AlCoCrNiMnV						
1. Grain boundary phase	15.5	16.1	12.6	22.7	19.1	14.0
2. Grain interiors	17.4	16.3	18.0	15.6	15.5	17.2

Mechanical properties

The engineering stress – engineering strain tensile curves of the AlCoCrNiMn and AlCoCrNiV alloys in the as-solidified conditions are given in Fig. 3. The respective tensile properties, such as yield stress (σ_y), ductility (ε_p), and volume fracture are given in Table 2. The stress-strain curves of the AlCoCrNi and AlCoCrNiV alloys as-solidified states clearly demonstrate significant capability of strain hardening and thus good overall ductility. The elongation to fracture of the base alloy is 83–87% and that of the AlCoCrNiMn alloy is 68–71%. Slightly lower ductility of the AlCoCrNiMn alloy in comparison with the AlCoCrNi alloy corroborates well with higher yield strength, because the ultimate tensile strengths and strain hardening coefficients of these alloys are comparable. The tensile behavior of the AlCoCrNiMn alloy is distinctively different from that of the two above-mentioned alloys. This alloy less exhibit plastic deformation at all, and demonstrates brittle fracture at the stress values.

The compression engineering stress–engineering strain curves are given in Fig. 4. For the sake of comparison the data on compressive behavior of the base AlCoCrNi alloy is also included. The base AlCoCrNi alloy demonstrates relatively

low yield stress, high ductility and high strain hardening; its strength increases and it shows no signs of cracking after compressive deformation of 75%. Compression test showing that yield strength of AlCoCrNiV between 1753 and 2381, but plasticity was decreased from 16.71 to 1.06. Alloying with V results in very significant strengthening of σ_y and ε_p. Strengthening is accompanied with the loss in the compression ductility down to 2.5%. An addition of Mn promotes a further increase in strength. We could not do compression test for HEAMn, because sample was very brittle. Compression test showing that yield strength of AlCoCrNiV between 1532 and 1856, but plasticity was decreased from 16.71 to 0.86 However, the compression ductility of this alloy is very low, only 0.5%.

Table 2

Tensile properties of (1) AlCoCrNiV and (2) AlCoCrNiMn alloys as-solidified conditions.

Compositions	**σ_y**	**ε_p**	**Volume fracture**	
	(MPa)	**(%)**	**Matrix (%)**	**Dendrite(%)**
HEA	1753	16.71	40	60
HEA-V2	2009	14.18	58	42
HEA-V4	2064	13.84	57	43
HEA-V6	2086	6.95	61	39
HEA-V8	2046	1.06	64	36
HEAV	2381	1.34	24	76

(1)

Compositions	**σ_y**	**ε_p**	**Volume fracture**	
	(MPa)	**(%)**	**Matrix (%)**	**Dendrite(%)**
HEA	1753	16.71	40	60
HEA-Mn2	1724	10.76	57	43
HEA- Mn4	1786	8.26	59	41
HEA- Mn6	1856	7.81	60	40
HEA- Mn8	1532	0.86	63	37
HEAMn	Brittle	Brittle	67	33

(2)

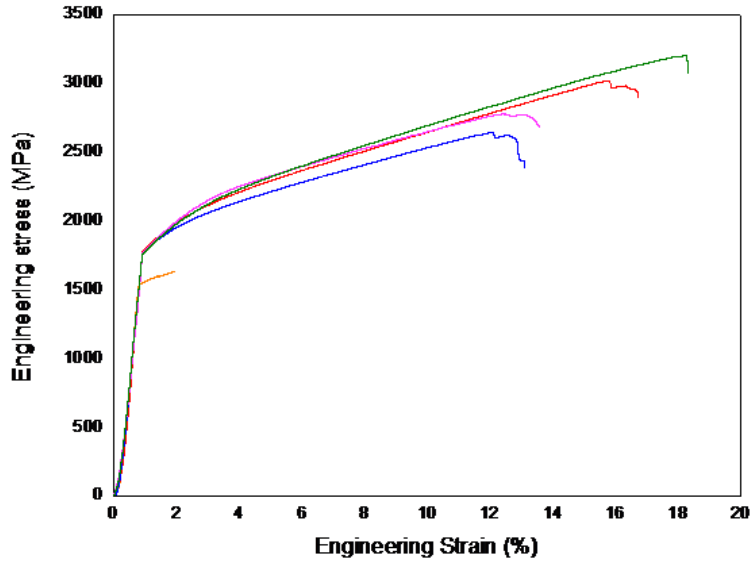

(a)

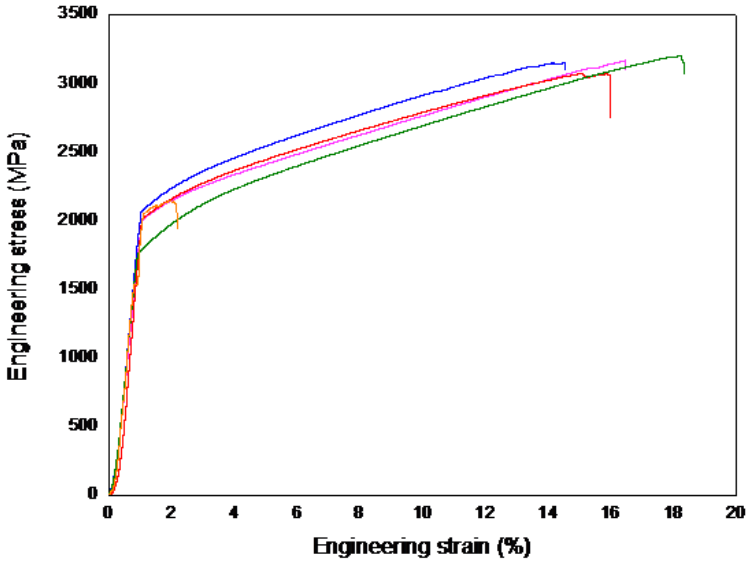

(b)

Fig. 3. Engineering strain of: a) AlCoCrNiMn and (b) AlCoCrNiV.

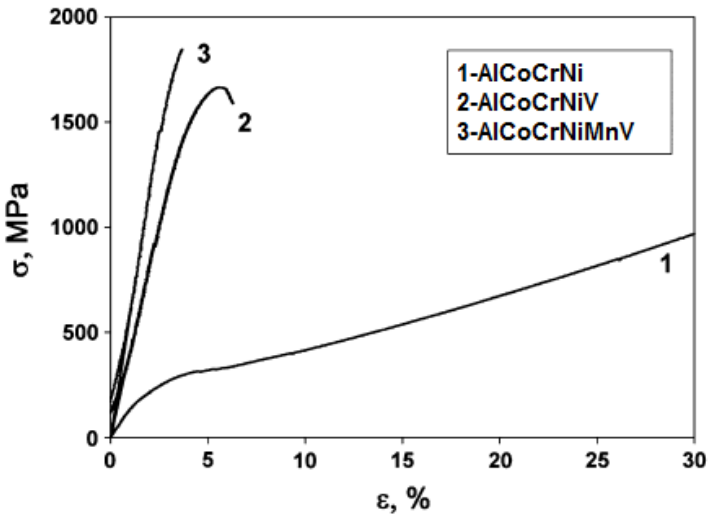

Fig. 4. Stress-strain curves obtained during compressive testing of the AlCoCrNi, AlCoCrNiV and AlCoCrNiMnV.

4.3. Discussion

Relationship between the microstructure and mechanical properties in $AlCoCrNiMn_xV_y$ alloys

The tensile testing results of the AlCoCrNi and AlCoCrNiMn alloys reported in this work are in good agreement with previously reported properties. Both alloys demonstrate very high ductility during tensile and compressive testing at room temperature. Very good ductility is likely caused by their dual-phase BCC solid solution structure. The yield strength of the AlCoCrNiMn alloy is slightly higher than that of the AlCoCrNi alloy, but ductility shows opposite behavior (δ = 68% in as-solidified state and δ = 71%). Higher strength of the Mn-containing alloy has also been reported by Gali and George and this is possibly related with strengthening effect from Mn due to more complex interactions of atoms in the 5-element solid solution. In accord to, these stresses are proportional to deviations of atomic radii δr_i and deviations of shear modulus δG_i. After test we could be seen that Mn brings very low deviations of atomic radii and shear modulus, and the strongest obstacles in these alloys are Cr atoms. Therefore, no strengthening of the AlCoCrNi alloy should be expected from the addition of Mn. Different grain size and different grain boundary composition environment may also affect the strength of the alloys; however, the limited set of the experimental data produced for these alloys does not allow us to make any statements on this issue.

The V-containing alloys are composed from two phases with distinctively different mechanical properties – the BCC solid solution, which is soft and ductile, and the B2 σ phase, which is hard and brittle. In such ‘‘composite’’ materials mechanical properties usually follow rule of mixtures, i.e. are determined as the volume-fraction averaged properties of individual phases. In the homogenized state, the volume fraction of the BCC/B2 phase is 41% and 27% in the AlCoCrNiV and AlCoCrNiMnV alloys, respectively.

The V-containing alloys are very brittle during tensile testing and also show little ductility during compression testing, especially the AlCoCrNiMnV alloy. The

matrix σ phase is known to be very brittle, and this behavior is demonstrated by the alloys. At the same time, the compression strength of these alloys is very high, σ_y = 1753 MPa for the AlCoCrNiV alloy and σ_y = 2002 MPa for the AlCoCrNiMnV alloy. The strength of the alloys is also expected to follow the rule of mixture, however, we have not been able to find any data on compressive properties of the stand-alone σ phase (most possible due to its brittleness). However, one can check the validity of the rule of mixtures by comparing calculated values of σ_y of the σ phase in two different alloys which could be easily determined. In these calculations, we have assumed that the strength of the BCC/B2 phase is σ_y = 1753 MPa, in accord with the value obtained during compression testing of the AlCoCrNi alloy. Using the known volume fractions of the σ and BCC/B2 phases and experimental σ_y values for the alloys, the calculations have returned $\sigma_y \approx 2064$ MPa and $\sigma_y \approx 1786$ MPa for the σ phase in the AlCoCrNiV and AlCoCrNiMnV alloys, respectively. These values are very close to each other, as it was expected from the comparison of the microhardness of the σ phase in the alloys. So one could say that the strength of the V-containing alloys also follows the rule of mixtures, and the higher strength of the AlCoCrNiMnV alloy is attributed to the higher volume fraction of the σ phase. Slightly higher ductility of the AlCoCrNiV alloy (ε = 2.5%) in comparison with the AlCoCrNiMnV alloy (ε = 0.5%) is probably associated with a higher volume fraction of the ductile BCC/B2 phase. Therefore one can suggest that relative fractions of the σ and BCC/B2 phases determine mechanical properties of these alloys.

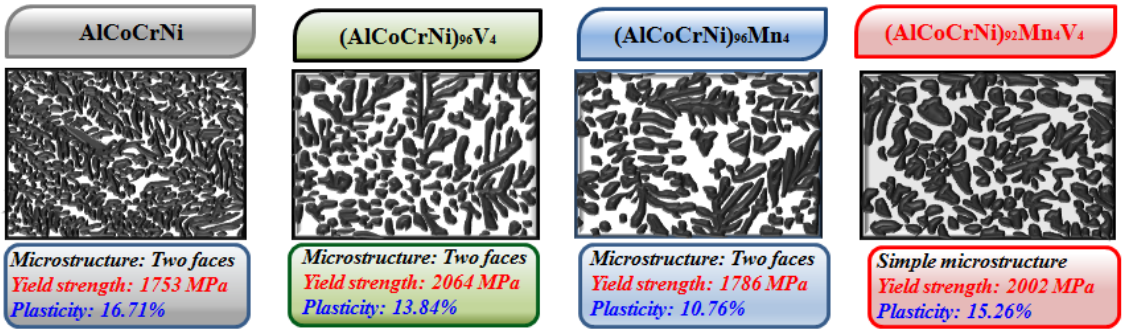

SECTION V

ECONOMY

Economical part

As the science of decision-making, economic philosophy operates in our daily lives whether we realize it or not. When we are evaluating the interest rates on our credit cards or trying to decide whether to buy or lease a new car or go out to dinner or on vacation, these are all decisions we make using economic thinking. We live in a world of limited resources, and economics helps us decide how to use these limited inputs to satisfy our never-ending list of wants and needs. Economics is also a large field with a rich history that's been explored and examined by hundreds of influential people, ranging from philosophers to politicians.

In its most simple and concise definition, economics is the study of how society uses its limited resources. Economics is a social science that deals with the production, distribution, and consumption of goods and services. Economics focuses heavily on the four factors of production, which are land, labor, capital, and enterprise. These are the four ingredients that make up economic activity in our world today and can each be studied individually.

I. Justification of technical–economical project.
II. Find volume of the investment.
III. Total cost of production per year.
IV. Calculations of time of the filing the expenses.

Table 1. Volume of the investment of the buying materials for production

№	Name	Quantity	Price (sum)	VAT 20%	Total price with VAT
1	Paper	1	20000	4000	24000
2	Disk	1	800	160	960
3	Chancellery	-	25000	5000	30000
4	Cartridge	1	12000	2400	14400
	Total				69360

Table 2. Volume of the cheap investment, building materials and the measuring instruments

№	Name	Quantity	Price (sum)	VAT 20%	Total price with VAT
1	Computer	1	1287000	257400	1544400
2	Printer	1	873000	167400	1004400
	Total				2548800

Table 3. Prices of the main funds

№	The name of main funds	The price of main funds
1	Laboratory	2100000
2	Measuring instruments	1110000
	Total	3210000

Share of the amortization 20%

$$Ash = 20\%* MF$$

$$Ash = 0.2 * 3210000$$

$$Ash = 642000 \text{ sum}$$

Main fund expenses for technical maintenance and repair of this year, forms 12%.

$$Prep = 12\% * MF$$

$$Prep = 0.12 * 3210000$$

$$Prep = 385200 \text{ sum}$$

Table 4. Plant expenditure budget

Expenditure types	Cost in sum
Engineer, technologist and worker's primary and additional salary	32168,74
Social insurance expenses (25%)	8042,19
Basic funds amortization	5921000

Repairing basic funds (10%)	3216,87
Safety engineering expenses (15%)	4825,31
Other expenditure of plant (7%)	2251,81

The main salary – It is found by means of salary all workers and their 40% bonus money.

Main s = salary * 0.4 + salary

Main s =1624664 * 0.4 +1624664

Main s = 2274529.6 sum

Expenses for insurance forms 25 % main salary

Pins =25% * Main s

Pins =0.25 * 2274529.6

Pins = 568632.4 sum.

Expenses for electricity

W = N*T*S

N- voltage kVt

T- time of the work

S- amount 1 kVt energy 228.60 sum

Energy expenses of the computer 1 kVt / hours

Energy expenses of the laboratory equipments 128 hours

W = 1 * 128 * 228.60 = 29261 sum.

Table 5.Total cost of production per year

№	Name of the cost	Unit Measurements (sum)	Amount	The share of expenses from total amount of expenses %
1	Expenses raw	1000 sums	10346,35	3,2
2	Amount of Annual Amortization	1000 sums	4775000	66,25
3	Wage fund	1000 sums	32168,74	3,17

4	Costs of social insurance	1000 sums	8042,19	4,87
5	Electricity consumption	1000 sums	15346	2,89
6	Consumption of materials	1000 sums	9331,38	19,49
	Total		4850234,66	100

The profitability

$$P= E/C * 100$$

$$P = 2977440 / 3213342.56 * 100$$

$$P = 92 \%$$

P – Profitability

E - Capital cost effectiveness

C – Capital

Calculations of time filing expenses.

$$Cexp = C/E$$

$$Cexp = 32133342.56/2977440=1.07$$

$$Cexp = 1 \text{ month}$$

SECTION VI

TECHNICAL SAFETY

Technical safety

Technical safety is an extensive system of factors guaranteeing that society can function smoothly and without disruptions. It aims at the safety of products on sale, trouble-free operation of industrial plants and the prevention of accidents caused by explosives.

Technical safety covers e.g. the safety of products and technical systems. It also includes the legislation and supervision by the authorities related to some other requirements, the verification of the required competences of controlling agencies, standardization, the safety of industrial plants that manufacture dangerous substances and their storage facilities, the verification of measurements, and metrology**.**

In this diploma work have been done with special laboratory equipment "Arc Melt Furnace ABJ-338" (Vacuum arc casting equipment) to fabricate HEA. Dimension of the equipment is small (1406 x 704 x 610mm) and operated by using electricity, argon and water. Water circulation constantly keeps cold condition. And it gives rapid cooling condition for HAE.

Safety instructions are described below:

- A hood vented to the outside is needed to remove vacuum pump oil fumes and any traces of metal that may be vaporized in the melting process;

- Lethal voltages are present at the power supply terminals. Lethal voltages are present on the outer surfaces of the vacuum equipment. The full power supply potential exists between the stinger arm and all other outside surfaces on the vacuum equipment. The stinger arm is the negative pole and all other metal components in and on the vacuum equipment are of the positive pole;

- A welding shade filter must be used over any viewing-port during arc melting or eye damage may result. Minimum 12 filters are needed and will work for lower currents. As currents exceed approximately 150 amps. For it 14 filters needed;

- Servicing, cleaning, setting up and using vacuum equipment requires the use of solvents, acids and power tools. Safety procedures for using these items should be known and strictly followed.

A person who works with this laboratory equipment does not pose any harm to his/her health, as the vacuum system and electricity operate in closed environment.

To work with the vacuum equipment one is required to wear:

- Laboratory glasses;
- White robe;
- Laboratory gloves.

SECTION VII

ECOLOGY

Ecological part

Industrial ecology aims to reduce the environmental impact of industry by examining material and energy flows in products, processes, industrial sectors, and economies. Industrial ecology provides a long-term perspective, encouraging consideration of the overall development of both technologies and policies for sustainable resource utilization and environmental protection into the future. It emphasizes opportunities for new technologies and new processes, and those for economically beneficial efficiencies. Industrial ecology draws on and extends a variety of related approaches including systems analysis, industrial metabolism, materials flow analysis, life cycle analysis, pollution prevention, design for environment, product stewardship, energy technology assessment, and eco-industrial parks.

Greater material efficiency, the use of better materials, and the growth of the service economy can contribute to the "dematerialization" of the economy. Resources that are cheap, abundant, and environmentally benign may be used to replace those that are expensive, scarce, or environmentally harmful. Such a substitution can be seen in the many important changes in energy sources that have occurred over the past century. As the energy sources have shifted from wood and coal toward petroleum and natural gas, the average amount of carbon per unit energy produced has decreased significantly, resulting in the "decarbonization" of world energy use.

Industrial ecology is concerned with the shifting of industrial process from linear (open loop) systems, in which resource and capital investments move through the system to become waste, to a closed loop system where wastes can become inputs for new processes.

Much of the research focuses on the following areas:

- material and energy flow studies
- dematerialization and decarbonization
- technological change and the environment

- life-cycle planning, design and assessment
- design for the environment
- extended producer responsibility
- eco-industrial parks
- product-oriented environmental policy
- eco-efficiency

Industrial ecology seeks to understand the way in which industrial systems (for example a factory, an ecoregion, or national or global economy) interact with the biosphere. Natural ecosystems provide a metaphor for understanding how different parts of industrial systems interact with one another, in an "ecosystem" based on resources and infrastructural capital rather than on natural capital. It seeks to exploit the idea that natural systems do not have waste in them to inspire sustainable design.

As I mentioned before, to prepare our composition we have been fabricated the alloy by small laboratory condition using arc melter under argon atmosphere. Therefore, probability of additional waste is very low. However, the elements that used for the alloys such as Aluminum (Al), Chromium (Cr), Cobalt (Co), Nickel (Ni), Vanadium (V), Manganese (Mn) are pure which means 99,99%. And this AlCoCrNiMnV high-entropy alloy melted without any waste.

State of the art process control allows get needed alloys safe way. So, as the experiment is conducted in a vacuum space whereas no damage to the person or nature whatsoever. Working on Vacuum arc casting laboratory equipment had no waste fumes or smell any gas.

SECTION VIII

CONCLUSION

Conclusion

The conclusion of the results shows that the research was mainly occurred by changing in microstructure and mechanical properties. During the experimental process, we try to add various amount of Vanadium (V) to AlCoCrNi composition and as a consequence, we controlled yield strength of the alloy. But the study shows that as while increasing amount of minor element, the plasticity started to decrease. However, effect of small amount of Manganese (Mn) increased plasticity even when we added with V as well. For example, when 4 at.% of Manganese alloyed with AlCoCrNiV (which includes 4 at.% of Vanadium), yield strength of this composition has not changed but plasticity increased. There was no change in microstructure in compositions whose mechanical properties were checked. But, we witnessed the change of volume fracture. During the experiment, the microstructure of the compositions showed two faces.

Among the analyzed compositions, in $AlCoCrNiMn_4V_4$, which is composed of six elements, the yield strength and plasticity were better than others and we have to take into account that this composition has six elements. Furthermore, the development of the $AlCoCrNiMn_4V_4$ HEA with remarkable mechanical properties at wide temperature ranges can contribute to extending the potential of dual-phase HEAs for structural applications. So, this composition can be used in various purposes and industries such as heavy industries.

REFERENCE

Reference

1. Sh.M. Mirziyoev: We will continue our path of national development with determinate and go up a new level, Tashkent: Uzbekistan, 2017 - 592 p.

2. Elyorjon Jumaev, S.H. Hong, J.T. Kim, H.J. Park, Y.S. Kim, S.Ch. Mun, J.Y. Park, G. Song, J.K. Lee, B.H. Min, T. Lee, Ki Buem Kim:Journal of Alloys and Compounds 777 (2019), p. 828-834.

3. D.B. Miracle, O.N. Senkov: A critical review of high entropy alloys and related concepts, Acta Mater. 122 (2017), p. 448-511.

4. J.W. Yeh, S.K. Chen, S.J. Lin, J.Y. Gan, T.S. Chin, T.T. Shun, C.H. Tsau, S.Y. Chang: Nanostructured high-entropy alloys with multiple principal elements: novel alloy design concepts and outcomes, Adv. Eng. Mater. 6 (2004), p. 299-303.

5. J.W. Yeh: Recent progress in high-entropy alloys, Ann. Chim. Sci. Mat. 31(2006), p. 633-648.

6. M.H. Tsai, J.W. Yeh: High-entropy alloys: a critical review, Mater. Res. Lett. 2(2014), p. 107-123.

7. Y. Zhang, T.T. Zuo, Z. Tang, M.C. Gao, K.A. Dahmen, P.K. Liaw, Z.P. Lu: Microstructures and properties of high-entropy alloys Progress in Materials Science 61 (2014), p. 1-93.

8. Cantor B., Chang I.T.H, Knight P., Vincent A.J.B: Microstructural development in equiatomic multicomponent alloys. Mater SciEng, A 2004; p. 375–377: 213-8.

9. Ma D., Tan H., Zhang Y., Li Y.: Correlation between glass formation and type of eutectic coupled zone in eutectic alloys. MaterTrans2003;44(10):2007-10.

10. Y.P. Wang, B.S. Li, M.X. Ren, C. Yang, H.Z. Fu: Microstructure and compressive properties of AlCrFeCoNi high entropy alloy, Materials Science and Engineering A 491 (2008), p. 154-158.

11. P.S. Sultonov: Ecology, Study guide book, p.50-68 .

12. X. Raximova: Occupational safety and health, Study guide book, p.81-89.

13. G.Yormatov: Occupational safety and health, Study guide book, p.38-42.

14. T.T. Juraev: Theory of economic, Study guide book, p.111-121 .
15. www.journals.elsevier.com
16. www.journals.indexcopernicus.com

APPENDIX